

# GeoFocus: Blending Efficient Global-to-Local Perception for Multimodal Geometry Problem-Solving

Linger Deng, Yuliang Liu\*, Wenwen Yu, Zujia Zhang,  
Jianzhong Ju, Zhenbo Luo, Xiang Bai

arXiv:2602.08524v1 [cs.CV] 9 Feb 2026

**Abstract**—Geometry problem-solving remains a significant challenge for Large Multimodal Models (LMMs), requiring not only global shape recognition but also attention to intricate local relationships related to geometric theory. To address this, we propose GeoFocus, a novel framework comprising two core modules. 1) Critical Local Perceptor, which automatically identifies and emphasizes critical local structure (e.g., angles, parallel lines, comparative distances) through thirteen theory-based perception templates, boosting critical local feature coverage by 61% compared to previous methods. 2) VertexLang, a compact topology formal language, encodes global figures through vertex coordinates and connectivity relations. By replacing bulky code-based encodings, VertexLang reduces global perception training time by 20% while improving topology recognition accuracy. When evaluated in Geo3K, GeoQA, and FormalGeo7K, GeoFocus achieves a 4.7% accuracy improvement over leading specialized models and demonstrates superior robustness in MATHVERSE under diverse visual conditions. Project Page – <https://github.com/dle666/GeoFocus>

**Index Terms**—Geometry problem solving, Large multimodal model, Geometry visual perception.

## I. INTRODUCTION

**G**EOMETRY Problem-Solving (GPS) involves analyzing shapes, reasoning about spatial relationships, and applying mathematical theories. These skills are fundamental to mathematics education [19] and play critical roles in various fields, including architecture [7], [8], mechanical engineering [47], [52], and robotic navigation [46]. With the advancement of Large Multimodal Models (LMMs) technology, researchers have begun to explore their potential in solving complex geometry problems.

Large Language Models (LLMs) [33], [14], [60] have demonstrated remarkable reasoning abilities, particularly in solving text-based mathematical problems. However, LMMs [18], [9], [41] face significant challenges in addressing multimodal mathematical geometry problems. These problems require models not only to comprehend textual information but also to perceive global geometric diagrams and integrate critical local details related to geometric theories. Although LMMs exhibit notable effectiveness in general visual question-answering tasks [23], [38], their training primarily relies on

L. Deng, W. Yu, Z. Zhang, Y. Liu, and X. Bai are with the School of Artificial Intelligence and Automation, Huazhong University of Science and Technology, Wuhan, 430074, China.

J. Ju and Z. Luo are with MiLM Plus, Xiaomi Inc, Beijing, 100000, China.  
Corresponding author: Y. Liu.

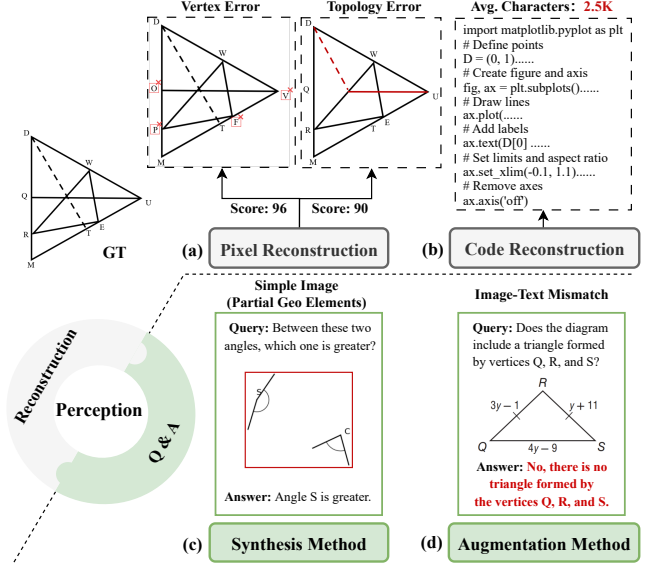


Fig. 1. The existing two paradigms for enhancing geometry perception of LMMs: image reconstruction and perception Q&A data generation.

datasets containing images of natural scenes. Such datasets lack geometric characteristics and fail to meet the visual perception demands required for solving geometry problems [57].

Recent studies on enhancing geometry visual perception in LMMs can be broadly divided into two categories, as shown in Fig. 1. The first category focuses on image reconstruction tasks [6], [45], which aim to improve the global understanding of topology structures in geometry images. Pixel-based reconstruction approaches emphasize accurate localization of pixels and color values but struggle with maintaining consistent vertex annotations and topology structures, as shown in Fig. 1 (a); code-rendering-based reconstruction approaches better preserve topology structures, but their high complexity requires 2,500 characters per image reconstruction, as shown in Fig. 1 (b). The second category is methods that generate perception question-answering (Q&A) data, which improve perception abilities through Q&A pairs training. However, data synthesis methods [58], [16] mainly produce images with simple components (Fig. 1 (c)) and fail to capture critical local features commonly found in reasoning images (e.g., midline, angle bisector). On the other hand (Fig. 1 (d)), dataset augmentation leveraging LMMs [12], [28] preserves

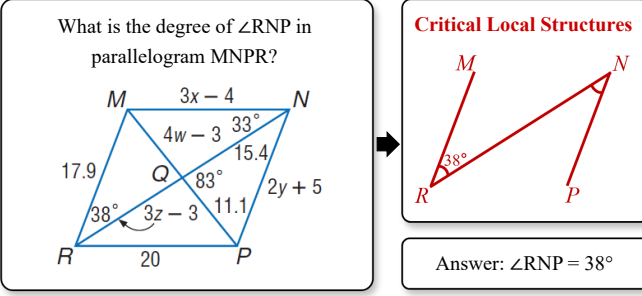


Fig. 2. Local structure with theoretical applicability is the key to geometry problem solving.

the complexity of the images, but the generated text often provides a global summary of the image and suffers from hallucination issues due to the perceptual limitations of LMMs. While existing methods effectively improve the global perception of geometric structures, they lack emphasis on local details, which contain critical theory information for solving problems. In contrast, humans prioritize these local details after grasping the overall structure when solving geometry problems, as shown in Fig. 2.

To address these issues, we propose GeoFocus, a method designed to enhance local visual perception abilities while maintaining improvements in global visual perception, aiming to strengthen the GPS ability of LMMs. GeoFocus consists of two core modules. The first module, Critical Local Perceptor, leverages thirteen theory-grounded perception Q&A templates to automatically identify and emphasize critical local information for GPS. This module achieves a 61% increase in critical local feature coverage compared to existing methods, enabling LMMs to sequentially extract critical local information in a human-like way before performing geometric reasoning. The second module is the VertexLang Topology Perceptor, which enables efficient global image reconstruction by designing a compact formal language, VertexLang, composed of vertex coordinates and topology connectivity relationships. Using VertexLang, geometric topology structure can be reconstructed with an average of only 0.3k characters, and the training time for global topology perception is reduced by 20% compared to code-based methods. This module emphasizes enhancing the model's global perception of topology structure.

Our contributions are summarized as follows:

- We introduce the Critical Local Perceptor, which automatically emphasizes critical local information using thirteen templates based on geometry theories. This expands critical local coverage by 61% over existing synthetic methods and enhances the ability to extract local key information similar to humans.
- We design a novel symbolic language, VertexLang, which represents geometric structures using vertex coordinates and topology connections for efficient global image reconstruction. It reduces training time by 20% compared to code-based methods while further improving global topology perception accuracy.
- GeoFocus achieves a 4.7% average improvement on three

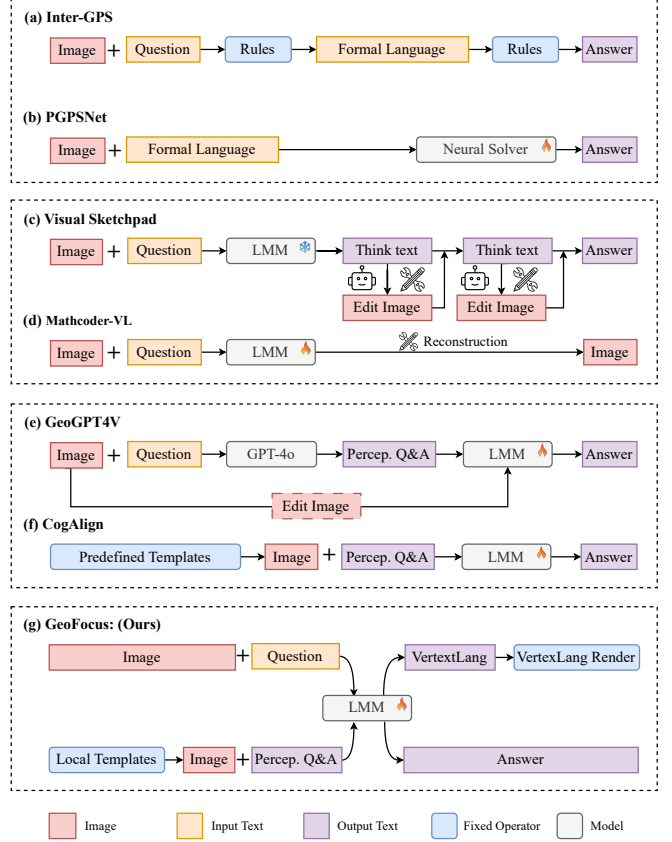


Fig. 3. Existing methods for improving GPS ability through visual perception, including formal language-based methods (a, b), image reconstruction-based approaches (c, d), and perception Q&A-based approaches (e, f). We propose GeoFocus (g), which enhances visual perception through global topology reconstruction and local perception Q&A training. ‘Percep.’ short for Perception.

GPS benchmarks compared to advanced geometric specialized LMMs and mitigates performance degradation caused by visual perception limitations on the MATH-VERSE benchmark.

## II. RELATED WORK

GPS is a long-standing yet challenging task in mathematics and has become a pivotal benchmark for evaluating the reasoning abilities of LMMs. Existing approaches to alleviate the visual perception limitation imposed on GPS performance can be grouped into three broad categories. Formal language-based methods, developed before the advent of LMMs, focus on translating geometric images into symbolic or otherwise more perceivable formats. In contrast, image reconstruction methods and perception Q&A approaches focus on enhancing LMMs' geometric diagram perception abilities through reconstruction or perception-focused Q&A training to improve their performance in GPS.

### A. Formal language-based methods

Formal language-based methods can be divided into two primary categories (Fig. 3 (a, b)). Rule-based methods [27], [34], [49], [36] first convert geometric diagrams into formal symbolic descriptions, then perform logical reasoning via

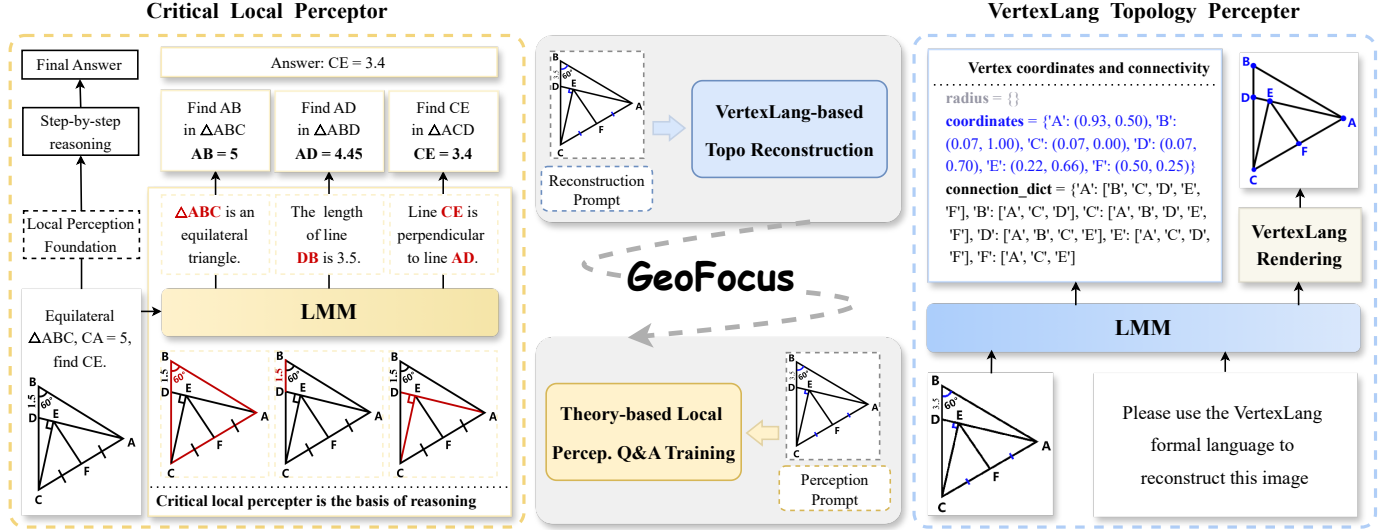


Fig. 4. Overview of the GeoFocus. Critical Local Perceptor focuses on the critical local structures required for GPS through perception Q&A training, laying the foundation for accurate reasoning. VertexLang Topology Perceptor improves the model’s understanding of topology structures through VertexLang-based Image Reconstruction training. ‘Percep.’ short for Perception.

path search. Although they perform strongly in constrained settings, their heavy dependence on handcrafted parsing rules limits generalization. Neural network-based methods integrate learned solvers for reasoning tasks. For instance, NGS [4] and Geoformer [3] enhance performance through self-supervised tasks, while PGPSNet [56] and LANS [22] combine structural and semantic information with specialized decoders. However, these methods are often tailored to specific datasets, which restricts their applicability to broader GPS tasks. Recent works [50], [55] alleviate this limitation by introducing LMM or more general symbolic languages, but the accuracy of converting images to symbolic representations remains a performance bottleneck.

### B. Image reconstruction methods

Image reconstruction-based methods can be broadly categorized into two paradigms (Fig. 3 (c, d)). The first paradigm [62], [15], [30] incorporates external tools during chain-of-thought (CoT) reasoning to reconstruct geometric images, which serve as reasoning steps to enhance spatial understanding. While effective for capturing complex geometric relationships, this paradigm introduces additional computational overhead during inference and requires robust perceptual abilities for effective image utilization. The second paradigm [45], [6], [48] integrates the image reconstruction task during training. Pixel-based reconstruction [6] and equal-length segment decomposition approaches [48] prioritize coordinate precision but demonstrate limited ability in focusing on geometric topology. Recently, code-based reconstruction methods [45] have shown great potential to enhance topological understanding through parametric representations, though they require a substantial text length (averaging 2.5k characters per image reconstruction).

### C. Perception Q&A methods

Perception Q&A methods aim to enhance the model’s perception abilities by training on specialized perception Q&A datasets, and can be grouped into two paradigms (Fig. 3 (e, f)). The first employs LMMs to expand existing data: [28] and [12] enrich Q&A pairs with CoT rationales; [39] and [33] synthesize new questions for existing geometric diagrams; and [2] integrates LMMs with computational geometry tools to simultaneously refine diagrams and generate questions, improving visual diversity. These methods effectively expand the data, but the generated Q&A pairs primarily focus on global perception and are limited by LMMs’ geometric hallucination. The second paradigm utilizes template-based generation: [16], [58], and [20] employ templates to ensure geometric data precision, but are constrained to elementary shapes with limited critical local information coverage. [31] and [11] combine formal language systems with templates to diversify question forms, but are still constrained by the limited template variety. Although templates guarantee correctness, the resulting synthetic data lacks the structural richness and complexity required for advanced GPS scenarios.

To further enhance the perception abilities of LMMs, we propose a novel approach, GeoFocus, as shown in Fig. 3 (g). By introducing theory-driven critical local perception Q&A training, and an efficient image reconstruction paradigm based on our sophisticatedly designed formal language, VertexLang, GeoFocus enables LMMs to better focus on critical local information related to theoretical knowledge after improving global perception.

## III. METHOD

To overcome the model’s GPS abilities limitations due to inadequate perception, we propose GeoFocus, which enhances geometry perception abilities through two core modules, as

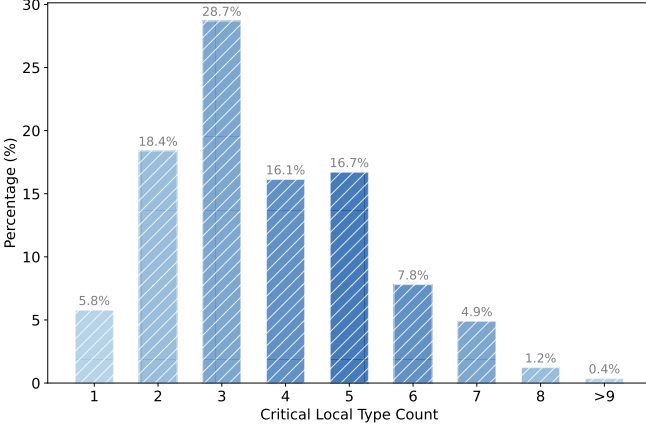


Fig. 5. Critical local structure type count percentage distribution in the classic GPS Q&A pairs.

illustrated in Fig. 4. The first module, Critical Local Perceptor, is designed to automatically emphasize critical local information by training on noise-free perception Q&A pairs instantiated from 13 local perception templates. This module imitates the human ability to focus on critical local information when solving geometry problems, which will be introduced in Sec. III-A. The second module, VertexLang Topology Perceptor, focuses on improving global structural understanding through image reconstruction training using a novel formal language, VertexLang, which will be introduced in Sec. III-B.

#### A. Critical Local Perceptor

When solving geometry problems, humans tend to focus on local structures that contain crucial information after forming an overall perception of the geometric diagram. Inspired by this observation, we proposed the Critical Local Perceptor, a module that defines 13 types of critical local structure based on geometric theory and common GPS data. For each structure type, we designed corresponding perception Q&A templates that guide the model to automatically identify and emphasize the local structures that are essential for solving the problem.

**Template Design.** We collected 5,000 middle-school geometry Q&A pairs based on the geometric theoretical framework, and distilled 13 categories of critical local structures necessary for reasoning (Fig. 8). The distribution of the number of critical local types employed in these pairs is shown in Fig. 5.

According to the distribution characteristics of collected data, we classify the critical local structures into two primary groups: Basic Measurement and Relational Reasoning. Basic Measurement emphasizes recognizing and comparing geometric quantities within critical local regions, focusing on numerical perception and the fundamental understanding of geometric concepts such as angles, lengths, and areas. Relational Reasoning, on the other hand, concentrates on identifying spatial relationships between geometric elements in critical local structures, including relationships between lines (e.g., parallel, perpendicular) and relationships between points and lines (e.g. collinear). To enable focus on each critical local structure, we design corresponding local perception Q&A

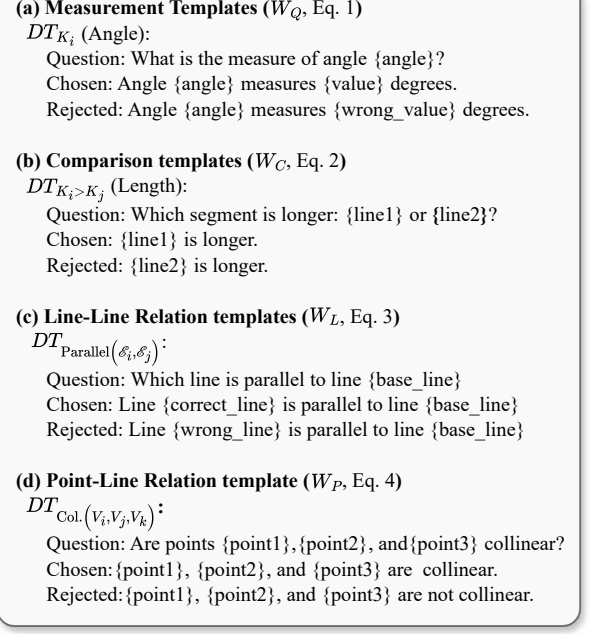


Fig. 6. Example of critical local perception Q&A generation template.

training template pools for two groups of local structure: the Basic Measurement Template Pool and the Relational Reasoning Template Pool, as shown in Fig. 7.

Let  $W$  represent the sub-pool of templates and  $DT$  represent a single data template. The Basic Measurement template pool contains two types of templates: quantification templates  $W_Q$  and comparison templates  $W_C$ . Let  $K$  denote the measurable properties of geometric objects such as angles, lengths, and areas. We define the quantification templates  $W_Q$  as:

$$W_Q(K_i) = DT_{K_i} \mid K_i \in [\text{Angle}, \text{Length}, \text{Area}], \quad (1)$$

representative template examples are shown in Fig. 6 (a). Comparison templates  $W_C$  between properties are expressed as:

$$W_C(K_i, K_j) = \begin{cases} DT_{K_i > K_j}, & \text{if } K_i \text{ is greater,} \\ DT_{K_i < K_j}, & \text{if } K_i \text{ is smaller,} \\ DT_{K_i = K_j}, & \text{if } K_i \text{ is equal,} \end{cases} \quad (2)$$

representative template examples are shown in Fig. 6 (b).

The Relational Reasoning template pool consists of Line-Line Relation templates  $W_L$  and Point-Line Relation templates  $W_P$ . Let  $\mathcal{E}$  represent the set of geometric lines. We define Line-Line Relation templates  $W_L$  as:

$$W_L(\mathcal{E}) = \begin{cases} DT_{\text{Shape}(\mathcal{E}_i, \dots, \mathcal{E}_n)}, & \text{if } \mathcal{E}_i, \dots, \mathcal{E}_n \text{ satisfy} \\ & \text{shape properties,} \\ DT_{\text{Bisector}(\mathcal{E}_i, \mathcal{E}_j, \mathcal{E}_k)}, & \text{if } \mathcal{E}_i \text{ bisects the angle} \\ & \text{between } \mathcal{E}_j \text{ and } \mathcal{E}_k, \\ DT_{\text{Parallel}(\mathcal{E}_i, \mathcal{E}_j)}, & \text{if } \mathcal{E}_i \parallel \mathcal{E}_j, \\ DT_{\text{Perpendicular}(\mathcal{E}_i, \mathcal{E}_j)}, & \text{if } \mathcal{E}_i \perp \mathcal{E}_j. \end{cases} \quad (3)$$

Line-Line Relation focuses on structural properties such as parallelism, perpendicularity, and angular bisectors, which are foundational prior knowledge of GPS. Representative template examples are shown in Fig. 6 (c). Let  $V$  represent the set of geometric points. We define Point-Line Relation templates  $W_P$  as:

$$W_P(V_i, \mathcal{E}_j) = \begin{cases} DT_{\text{Midpoint}(V_i, \mathcal{E}_j)}, & \text{if } V_i \text{ divides } \mathcal{E}_j \text{ into} \\ & \text{equal segments,} \\ DT_{\text{On-Circle}(V_i, \mathcal{E}_j)}, & \text{if } V_i \text{ lies on the} \\ & \text{circumference of } \mathcal{E}_j, \\ DT_{\text{Perp.-Foot}(V_i, \mathcal{E}_j)}, & \text{if } V_i \text{ is the perp.} \\ & \text{foot of } \mathcal{E}_j, \\ DT_{\text{Col.}(V_i, V_j, V_k)}, & \text{if } V_i, V_j, V_k \\ & \text{lie on the same line.} \end{cases} \quad (4)$$

Point-Line Relation emphasizes positional relationships such as collinear, perpendicular foot, and midpoint properties, which are critical for understanding geometric configurations. Representative template examples are shown in Fig. 6 (d). See the supplementary material for detailed templates.

**Perceptor Design.** To ensure accuracy while increasing the coverage of critical local in perception Q&A data, we propose Critical Local Perceptor based on the **Template Design**, as shown in Fig. 7. Following [58], [20], [9], we progressively obtain descriptions and geometric properties during the image generation process. Differing from these approaches, we design the Description Transformation Module and the Property Transformation Module, which match descriptions and properties with template pools to generate Q&A pairs related to critical local perception.

Specifically, the Property Transformation Module  $T_P(K)$  specializes in numerical problems and addresses the perception requirements by matching Basic Measurement Template Pool. During the generation process, the transformation function  $H_P$  maps all eligible property information into numerical perception problems:

$$T_P(K) = H_P(W_Q(K) \cup W_C(K_i, K_j)). \quad (5)$$

As shown in Fig. 7, for the property ‘Length:  $AB = 5.02$ ,  $AC = 5.02$ ’,  $H_P$  first matches the length category based on keyword ‘Length’, then matches the Comparison category based on the inclusion of multiple objects, and finally matches the equal template  $TC_{K_i=K_j}$  based on the value to obtain the corresponding Q&A pair.

The Description Transformation Module  $T_R(\mathcal{E}, V)$  focuses on relational problems and addresses the perception requirements by matching the Relational Reasoning Template Pool. The transformation function  $H_R$  maps the description information into relational reasoning problems:

$$T_R(\mathcal{E}, V) = H_R(W_L(\mathcal{E}_i, \mathcal{E}_j) \cup W_P(V_i, \mathcal{E}_j)). \quad (6)$$

For example, for the description ‘Point F is the midpoint of line segment AC’,  $H_R$  first matches the Point-Line category based on uppercase letters, and then matches the  $DT_{\text{Midpoint}(V_i, \mathcal{E}_j)}$  template based on the ‘midpoint’ keyword to obtain the

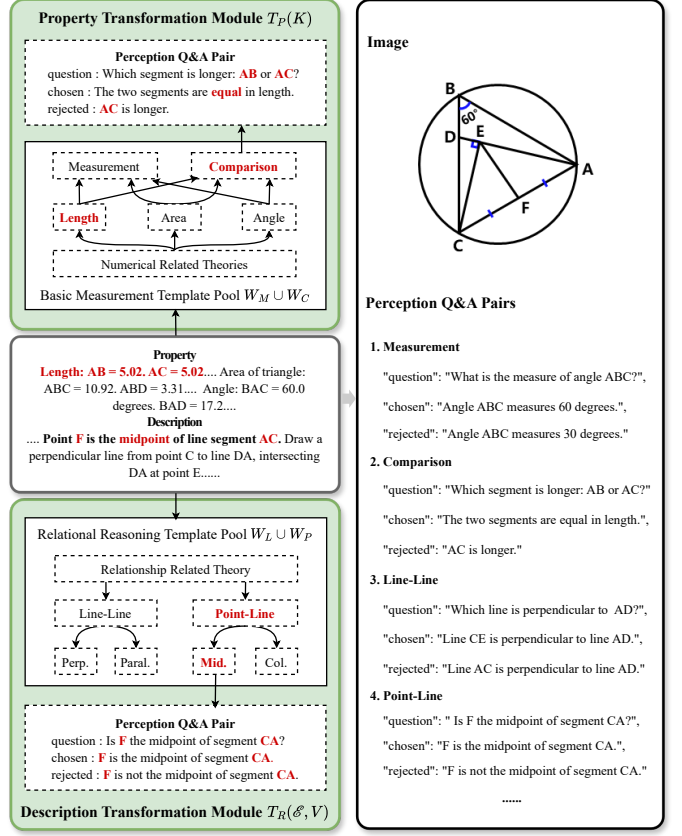


Fig. 7. Critical Local Perceptor extracts geometry properties and descriptions to generate numerical and relational Q&A pairs through the Property Transformation Module and Description Transformation Module.

corresponding Q&A pair. These templates are designed to enhance the perception of critical local structures, aligning with the definitions and inference mechanisms in geometric theories, thereby forming a foundational perception skill for GPS.

Representative examples from the Critical Local Perceptor are illustrated in Fig. 8, which includes thirteen question types. We employ these high-quality instructional samples for training, focusing on improving the model’s ability to perceive critical local information. Considering the diversity of answer formats, we adopt the Direct Preference Optimization (DPO) algorithm for training. The objective function of DPO is:

$$\mathcal{L}_{\text{DPO}} = -\mathbb{E}_{\mathbf{Q}, \mathbf{I}, \mathbf{R}^+} [\log P(\mathbf{R}^+ | \mathbf{Q}, \mathbf{I})] + \mathbb{E}_{\mathbf{Q}, \mathbf{I}, \mathbf{R}^-} [\log P(\mathbf{R}^- | \mathbf{Q}, \mathbf{I})], \quad (7)$$

where  $\mathbf{Q}$  represents a user query,  $\mathbf{I}$  denotes an input image,  $\mathbf{R}^+$  is a positive response, and  $\mathbf{R}^-$  is a negative response. Unlike supervised fine-tuning, which constrains the model’s output tokens and leads to an excessive focus on non-unique expressions, thereby impairing the model’s generalization ability. DPO imposes no strict constraints on the content of the model’s responses; instead, it optimizes the model by encouraging outputs to progressively approach the correct answer and diverge from incorrect ones. This sparse supervision avoids overemphasis on non-unique token expressions, effectively enhancing the model’s understanding of the relationships be-

Angle Value	Angle Compare	Length Value	Length Compare	Area Compare
Shape Check	Bisector Check			
Midpoint Check	On Circle			
		<b>Critical Local Q&amp;A Samples</b>		

Fig. 8. Critical Local Perceptor problem types and typical examples. Each example includes an image, a question, a correct answer aligned with the image, and an incorrect answer that conflicts with it.

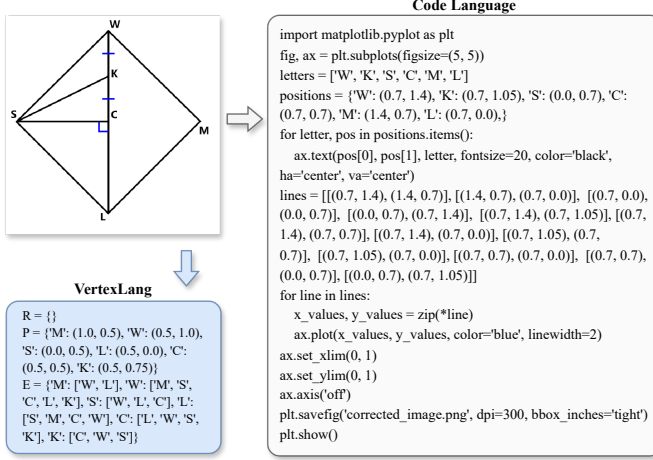


Fig. 9. Qualitative comparison of VertexLang-based and Code Language-based image reconstruction.

tween local structures and theories. This stage provides solid prior knowledge for subsequent symbolic reasoning.

### B. VertexLang Topology Perceptor

Global perception is a prerequisite for local perception, and its quality directly determines local perception performance. To improve reconstruction efficiency and emphasize global topology structures, we propose a novel formal language, VertexLang, which enables a new paradigm for image reconstruction.

1) *Definition of VertexLang*: We observed that the global topology information of geometry can be decomposed into sets of vertices and edges. Building on this observation, we propose VertexLang, a geometric formal language comprising a circle radius dictionary  $\mathbf{R}$ , a vertex coordinate dictionary  $\mathbf{P}$ , and a connectivity dictionary  $\mathbf{E}$  for efficient image reconstruction.

The radius dictionary  $\mathbf{R}$  is specialized for geometric images containing circle substrates, which is defined as:

$$\mathbf{R} = \{o_i : r_i | o_i \in \mathcal{O}, r_i > 0\}, \quad (8)$$

where  $o_i : r_i$  denotes a key-value pair in the dictionary,  $o_i$  represents center annotations,  $r_i$  represents the radius value, and  $\mathcal{O}$  is the set of centers. If no circle exists,  $\mathbf{R}$  remains empty. The vertex coordinate dictionary  $\mathbf{P}$  is defined as:

$$\mathbf{P} = \{v_i : (x_i, y_i) | v_i \in V, x_i \in [0, 1], y_i \in [0, 1]\}, \quad (9)$$

where  $V$  is the set of vertices,  $v_i$  represents vertex annotations, and  $(x_i, y_i)$  denotes the normalized coordinate value. All coordinates are normalized to emphasize relative positional relationships between vertices rather than absolute edge lengths. Finally, the connectivity relationship dictionary  $\mathbf{E}$  expressed as:

$$\mathbf{E} = \{v_i : \mathcal{N}(v_i) | v_j \in V, \mathcal{N}(v_i) = \{v_j | v_j \sim v_i, v_j \in V\}\}, \quad (10)$$

where  $\mathcal{N}$  is the power set of vertex set  $V$ ,  $v_j \sim v_i$  represents vertex  $v_j$  connected to vertex  $v_i$  via straight lines. During the image rendering stage,  $\mathbf{R}$ ,  $\mathbf{P}$ , and  $\mathbf{E}$  are input into a predefined image rendering function  $\mathcal{F}(\mathbf{R}, \mathbf{P}, \mathbf{E})$  to generate the unique geometry image  $G$ :

$$G = \mathcal{F}(\mathbf{R}, \mathbf{P}, \mathbf{E}). \quad (11)$$

VertexLang replaces procedural drawing sequences with a compact coordinate-connectivity dictionary representation for geometric topology reconstruction, removing tool-specific drawing code unrelated to image content, thereby reducing the character number required for reconstruction. Following the prompt in [45], we used Gemini-2.0-Flash (a model with high topological fidelity and fast, low-cost outputs) to generate code for 2,500 images covering the full complexity range, maintaining statistical power while keeping resource costs manageable. Through statistical analysis, we demonstrate that, on the same set of 2,500 images, reconstruction with VertexLang achieved an 88% reduction in comment character count compared to the

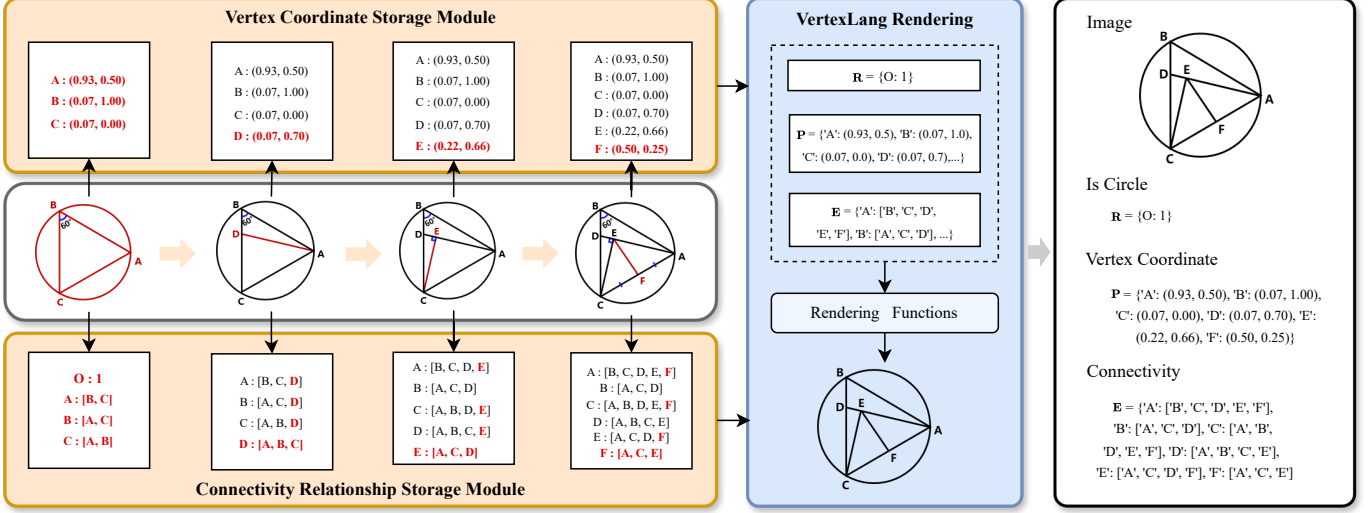


Fig. 10. The VertexLang Reconstructor determines the circle radius dictionary  $\mathbf{R}$  based on the selected substrate. As geometric elements are gradually added, the Vertex Coordinate Storage Module and the Connection Relationship Storage Module are updated to obtain the vertex coordinate dictionary  $\mathbf{P}$  and connectivity relationship dictionary  $\mathbf{E}$ , respectively. The final image is rendered via the Code Rendering.

### Algorithm 1: VertexLang Reconstructor

**Input:** Geometry substrate set  $\mathbf{S}$ , number of substrates  $n_1$ , number of vertices  $n_2$ , connectivity constraints  $\mathcal{C}$

**Output:** Rendered geometry image  $G$ , VertexLang text  $T$

**1 Initialization:**

- 2 radius  $\mathbf{R} \leftarrow \emptyset$
- 3 vertex dictionary  $\mathbf{P} \leftarrow \emptyset$
- 4 connectivity dictionary  $\mathbf{E} \leftarrow \emptyset$

**5 Subroutine: Add Vertex and Connectivity**

**6 Function**  $\text{AddVertex}(\mathbf{P}, \mathbf{E}, \mathcal{C})$ :

- 7  $(x, y) \leftarrow \text{generate normalized coordinates } \in [0, 1]$
- 8  $v \leftarrow \text{assign unique vertex annotation}$
- 9  $\mathbf{P} \leftarrow \mathbf{P} \cup \{v : (x, y)\}$
- 10  $\mathcal{N}(v) \leftarrow \{v_j | v_j \sim v, v_j \in V\}$  based on  $\mathcal{C}$
- 11  $\mathbf{E} \leftarrow \mathbf{E} \cup \{v \rightarrow \mathcal{N}(v)\}$

**12 Step 1: Substrate Selection**

**13 for**  $i \leftarrow 1$  to  $n_1$  **do**

- 14  $s_i \leftarrow \text{sample from } \mathbf{S}$
- 15 **if**  $s_i$  is a circle **then**
- 16  $r_i \leftarrow \text{determine radius of circle from } s_i$
- 17  $\mathbf{R} \leftarrow \mathbf{R} \cup \{o_i : r_i, o_i \in \mathcal{O}\}$
- 18  $\text{AddVertex}(\mathbf{P}, \mathbf{E}, \mathcal{C})$

**19 Step 2: Line Addition**

**20 for**  $i \leftarrow 1$  to  $n_2$  **do**

- 21  $\text{AddVertex}(\mathbf{P}, \mathbf{E}, \mathcal{C})$

**22 Step 3: Geometry Rendering**

**23**  $G \leftarrow \mathcal{F}(\mathbf{R}, \mathbf{P}, \mathbf{E})$

**24**  $T \leftarrow \mathbf{R}, \mathbf{P}, \mathbf{E}$

**25 return**  $G, T$

code-based method [45]. The qualitative example is shown in Fig. 9. Furthermore, leveraging this concise and efficient topological representation, VertexLang reduces training time by 20% compared to the code-based method [45].

2) *VertexLang Reconstructor*: To obtain appropriate samples for the VertexLang-based image reconstruction, we design a sample generation engine, VertexLang Reconstructor, as illustrated in Fig. 10.

Existing methods [9], [11] combine substrate selection with the progressive addition of specialized elements to generate images, but cannot produce VertexLang annotations. Therefore, to synthesize high-quality VertexLang annotations, we introduce a novel pipeline, VertexLang Reconstructor. The process begins by selecting substrates and determining whether a circular substrate is included. If a circular substrate is selected, it is used to construct the radius dictionary  $\mathbf{R}$ ; otherwise,  $\mathbf{R}$  remains empty. As geometry elements are added sequentially, their vertex coordinates  $(x, y)$  and connectivity relationships  $\mathcal{N}(v)$  are stored according to VertexLang syntax. Specifically, the Vertex Coordinate Storage Module maps each vertex label to the corresponding coordinate pair  $(x, y)$ , while the Connectivity Relationship Storage Module maps each vertex label to the list of adjacent vertex labels  $\mathcal{N}(v)$ . These mappings form two key dictionaries: the vertex coordinate dictionary  $\mathbf{P}$  and the connectivity dictionary  $\mathbf{E}$ . Finally, the dictionaries  $\mathbf{R}$ ,  $\mathbf{P}$ , and  $\mathbf{E}$  are fed into the Code Rendering Module, which employs a predefined algorithm to generate a unique geometry image. The pseudo-code outlining the pipeline of VertexLang Reconstructor is provided in Algor. 1.

## IV. EXPERIMENTS

### A. Setup

**Implementation Details.** We evaluated the effectiveness of our approach on different models, specifically Qwen2.5-VL-3B, Qwen2.5-VL-7B [1], and Gemma3-4B [42]. The learning

rate was set to  $10^{-7}$ . In the first stage, the VertexLang Topology Perceptor was trained for 15 epochs using the default EasyR1 [51] configuration, and in the second stage, the Critical Local Perceptor was trained for 1 epoch following the standard LlamaFactory setup [61]. Unless stated otherwise, all ablation studies are conducted on Qwen2.5-VL. The method is only employed during training, introducing no extra overhead at inference time.

**Benchmarks.** Experiments were conducted on three widely used multimodal GPS benchmarks: Geometry3K (Geo3K) [27], GeoQA [4], and FormalGeo7K [59]. Below is a brief overview of each test dataset: 1) GeoQA consists of 754 geometry questions sourced from Chinese secondary school exams. The images in this dataset are directly obtained by scanning exam papers, reflecting the visual characteristics of real-world GPS tasks. This dataset evaluates the model’s reasoning ability in natural scene geometry images. 2) Geo3K contains 601 geometry questions derived from example problems in secondary school textbooks, with manually annotated questions and answer options. The textual content of Geo3K is relatively concise, and most critical information for problem-solving is embedded in geometric images. Consequently, this dataset poses higher demands on a model’s visual perception abilities. 3) FormalGeo7K comprises 1,050 geometry problems collected from online resources and curated manually to ensure quality. It features a broad range of problem types to provide a comprehensive evaluation setting for GPS models.

We evaluated models’ geometric perception using the CogAlign-data [16] dataset, which comprises synthetic images paired with Q&A pairs across four core tasks probing geometric perception. Additionally, out-of-domain generalization was evaluated on four prominent multimodal mathematics datasets (We-Math [35], MathVerse [57], MathVision [44], and MathVista [26]), as well as the hallucination dataset Hallusion-Bench [13] and the graph reasoning dataset ChartQA [29].

**Training Strategy.** Due to the model’s weak initial performance in image reconstruction, RL algorithms struggle to efficiently identify optimization directions [54]. To accelerate convergence and improve training stability in early stages, we design a new training strategy, DynamicGT-RL, which dynamically replaces the model-generated policy with ground truth (GT) to guide the model toward the correct optimization trajectory. The incorporation of GT influences  $\hat{A}_i(R)$  calculation as follows:

$$\hat{A}_i(R(P)) = \begin{cases} \frac{R(p_i) - \text{mean}(R(P_{\text{model}}))}{\text{std}(R(P_{\text{model}}))}, & x \geq \tau, \\ \frac{R(p_i) - \text{mean}(R(P_{\text{model}} \cup P_{\text{gt}}))}{\text{std}(R(P_{\text{model}} \cup P_{\text{gt}}))}, & x < \tau, \end{cases} \quad (12)$$

where  $p_i$  is a policy,  $P$  is a set of policies,  $x$  is a random number between 0 and 1, and  $\tau$  indicates the GT replacement proportion. For the VertexLang-based image reconstruction task, we design a Reconstruction Reward  $R_{\text{recon}}$ , which consists of two components: vertex coordinate accuracy reward  $R_{\text{coord}}$  and connectivity relationship accuracy reward  $R_{\text{conn}}$ . Vertex coordinate accuracy reward is assessed by calculating the Euclidean distance between the model-predicted coordinates and the corresponding GT coordinates. Connectivity relationship accuracy reward is measured using the F1 score

$R_{\text{conn}}$ , which compares the model-predicted edge set with the GT edge set. The combined reward is calculated as follows:

$$R_{\text{recon}} = 0.5 * R_{\text{coord}} + 0.5 * R_{\text{conn}}. \quad (13)$$

Finally, we replace  $R$  in Eq. 16 with  $R_{\text{recon}}$  for the corresponding calculations. See the supplementary material for more details.

**Evaluation and Metrics.** To evaluate the model’s reasoning ability on the GPS dataset, we employ the EasyR1 [51] format script to extract open-ended answers and compute accuracy metrics. For the out-of-domain datasets, we utilize the evaluation scripts provided by NoisyRollout [24] to assess the accuracy. To evaluate the model’s image topology reconstruction ability, we render the model-generated outputs into images and convert them into structured language representations using FGeo-Parser [63]. These representations are then compared against the GT. Topology reconstruction quality is assessed using BLEU-4 [32] and Construction CdlAcc (Cons. CdlAcc) [63].

## B. Ablation Study

In Sec. IV-B1, we performed ablation on the overall architecture of GeoFocus to analyze the contribution of each module to GPS. Then, we ablation on the internal designs of the Critical Local Perceptor module (Sec. IV-B2) and the VertexLang Topology Perceptor module (Sec. IV-B3). Finally, Secs. IV-B4 and IV-B5 evaluate the effectiveness of GeoFocus across different baselines and analyze the impact of varying the order in which the modules are applied.

*1) Ablation of the proposed modules:* To evaluate the contribution of the VertexLang Topology Perceptor module and the Critical Local Perceptor module, we analyzed their effects in isolation and combination. As shown in the General LMM section of Tab. I, the reasoning performance of the General LMM improves when either module is employed independently. For example, in the 3B model, training with the VertexLang Topology Perceptor module or Critical Local Perceptor module on synthetic data resulted in a reasoning performance improvement on real-world data by 2.3% and 2.9%, respectively. This indicates that enhancing global topology perception and local understanding individually has a positive impact on the model’s reasoning ability. Furthermore, these foundational abilities generalize effectively to out-of-domain geometry datasets. When the VertexLang Topology Perceptor module and Critical Local Perceptor module are combined, the reasoning performance of the 3B and 7B models improved further by 5.4% and 4.1%, respectively. These results suggest that integrating the VertexLang Topology Perceptor and Critical Local Perceptor produces an additive effect through optimization within the parameter space.

Recently, Group Relative Policy Optimization (GPRO) [37] has emerged as a mainstream training paradigm for enhancing the symbolic reasoning abilities of LMMs. To further validate the effectiveness of GeoFocus on models with strong geometry symbolic reasoning performance, the GeoFocus-trained model was further optimized using the GPRO training paradigm on

TABLE I

ABLATION OF THE GEOFOCUS ON GENERAL LMMs AND GRPO-BASED GEOMETRY-SPECIFIC LMMs. ‘TOPO’ DENOTES THE VERTEXLANG TOPOLOGY PERCEPTER. ‘LOCAL’ DENOTES THE CRITICAL LOCAL PERCEPTOR. BOTH MODULES ARE TRAINED ONLY ON SYNTHETIC DATA.

	Topo	Local	Geo3K	GeoQA	Formalgeo7k	Total
General LMMs						
3B	✗	✗	25.3	32.1	16.8	74.2
	✓	✗	25.4	33.8	17.3	76.5 (2.3↑)
	✗	✓	25.6	34.2	17.3	77.1 (2.9↑)
	✓	✓	26.5	34.4	18.7	79.6 (5.4↑)
7B	✗	✗	39.4	44.4	35.6	119.4
	✓	✗	39.8	46.6	36.0	122.4 (3.0↑)
	✗	✓	40.1	46.2	35.6	121.9 (2.5↑)
	✓	✓	40.3	47.1	36.1	123.5 (4.1↑)
GRPO-based Geometry-specific LMMs						
3B	✗	✗	48.3	63.0	53.0	164.3
	✓	✗	48.9	63.3	54.5	166.7 (2.4↑)
	✗	✓	48.6	63.0	54.7	166.3 (2.0↑)
	✓	✓	50.4	64.3	55.4	170.1 (5.8↑)
7B	✗	✗	52.6	70.1	62.6	185.3
	✓	✗	55.2	71.8	63.4	190.4 (5.1↑)
	✗	✓	55.1	70.3	63.1	188.5 (3.2↑)
	✓	✓	55.3	71.9	63.7	190.9 (5.6↑)

geometric datasets. As shown in the GRPO-based Geometry-specific LMM section of Tab. I, consistent effectiveness is observed when symbolic reasoning training based on GPRO is incorporated. Models enhanced with GeoFocus for improved perception abilities maintain an advantage of 5.8% and 5.6% over models relying solely on symbolic reasoning. These findings support the hypothesis that image perception and symbolic reasoning represent distinct skills that can be optimized in parallel to improve GPS performance.

### 2) Ablation of the design in Critical Local Perceptor:

In this section, we perform ablation studies to analyze the necessity of improving the geometry critical local structure coverage, as well as the advantages of the Critical Local Perceptor compared to existing methods.

**Ablation of critical local structure coverage.** To evaluate the impact of expanded critical local structure coverage on perception Q&A data for GPS, we designed three experimental configurations. Specifically, we employed samples from the Critical Local Perceptor with varying levels of critical local structure coverage (40%, 70%, and 100%) for model training. As shown in Fig. 11, the overall performance of models consistently improves as local structure coverage increases. This indicates that expanding the critical local structure coverage in perceptual Q&A data can effectively enhance the model’s performance in GPS.

**Advantage of Critical Local Perceptor in improving perception performance.** We compare Critical Local Perceptor with the existing perception Q&A synthesis engine, CogAlign, under the same 65k data scale. As shown in Tab. II, the 3B and 7B models trained with the Critical Local Perceptor achieve an average improvement of 5.7% on the CogAlign-data test set compared to those trained on CogAlign’s native samples. We attribute this improvement to the broader coverage of local perception. Critical Local Perceptor encompasses thirteen

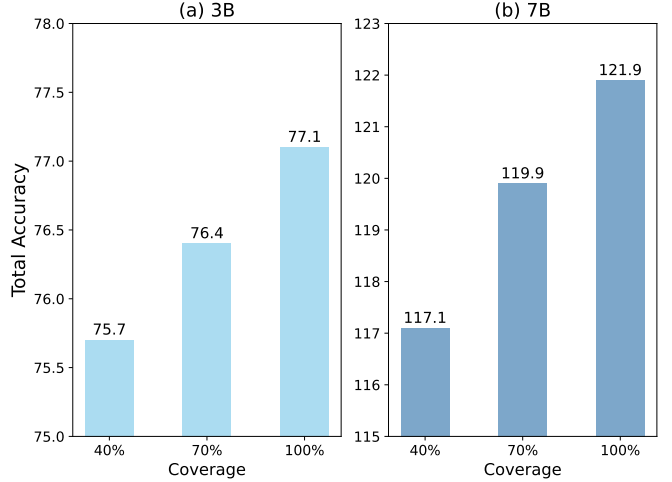


Fig. 11. The impact of critical local structure coverage on GPS performance. (a) Performance of the 3B model under varying levels of critical local structure coverage. (b) Performance of the 7B model under varying levels of critical local structure coverage.

local geometric perception tasks, closing the gap left by the CogAlign set of eight tasks. This more comprehensive set of local signals enables stronger cross-scene generalization. See the supplementary material for a detailed comparison of task types.

**Advantage of Critical Local Perceptor in enhancing reasoning performance.** We further evaluate the effectiveness of the Critical Local Perceptor in GPS. As shown in Tab. III, models trained exclusively on CogAlign show slight decreases in GPS performance (3B: -0.1%, 7B: -2.0%). In contrast, models trained with Critical Local Perceptor outperform the baseline by 1.4% (3B) and 2.0% (7B), respectively. This per-

TABLE II  
COMPARISON WITH THE SYNTHETIC GEOMETRY PERCEPTION Q&A METHOD COGALIGN ON THE COGALIGN-DATA PERCEPTION TEST SET.

	Configuration	Angle Comparison	Perpendicular Detection	Parallel Comparison	Chart Projection	Avg.
3B	Baseline	62.5	54.1	57.0	79.5	63.3
	CogAlign	70.1	55.7	49.6	83.4	64.7
	Local Perceptor	91.6	55.7	60.7	81.9	<b>72.5</b>
7B	Baseline	87.1	59.0	63.7	90.2	75.0
	CogAlign	84.6	60.1	68.7	90.2	75.9
	Local Perceptor	89.1	60.8	77.1	90.5	<b>79.4</b>

TABLE III  
COMPARISON WITH THE SYNTHETIC GEOMETRY PERCEPTION Q&A METHOD COGALIGN ON REAL-WORLD GPS DATASETS.

	Configuration	Geo3K	GeoQA	Formalgeo7k	Total
3B	Baseline	25.3	32.1	16.8	74.2
	CogAlign	25.5	31.6	17.0	74.1 (0.1↓)
	Local Perceptor	25.8	32.6	17.2	75.6 (1.4↑)
	CogAlign + Local Perceptor	26.5	34.9	16.8	78.2 (4.0↑)
7B	Baseline	39.4	44.4	35.6	119.4
	CogAlign	38.1	43.4	35.9	117.4 (2.0↓)
	Local Perceptor	39.1	46.3	36.0	121.4 (2.0↑)
	CogAlign + Local Perceptor	40.3	45.0	36.7	122.0 (2.6↑)

TABLE IV  
PERCEPTION Q&A TRAINING STRATEGY ABLATION EXPERIMENT. ‘SL’ REPRESENTS SUPERVISED LEARNING.

	Training	Geo3K	GeoQA	Formalgeo7k	Total
3B	SL	25.5	33.4	17.0	75.9
	DPO	25.6	34.2	17.3	77.1
7B	SL	36.6	44.3	33.7	114.6
	DPO	40.1	46.2	35.6	121.9

formance gap arises from CogAlign’s oversimplified images, which lack the complexity and distributional diversity essential for GPS. As a result, CogAlign-trained models acquire only basic perception skills but struggle to generalize to reasoning tasks. In contrast, we argue that the Critical Local Perceptor mitigates these limitations by integrating local perception tasks that are closely related to reasoning image, thereby improving the coverage of critical local regions by 61%. Furthermore, combining Critical Local Perceptor with CogAlign leads to additional improvements of 4.0% (3B) and 2.6% (7B), further demonstrating Critical Local Perceptor’s effectiveness in enhancing GPS abilities.

**Ablation of perception Q&A training strategy.** The comparison results of the perception Q&A training strategies are shown in Tab. IV. For the local perception Q&A tasks, models trained using DPO consistently outperform those trained with supervised fine-tuning. This difference may arise from the limitations of supervised fine-tuning, which embeds answers directly into the model, often hindering the model’s ability to prioritize key information and constrain generalization. In contrast, DPO requires the model to approach the correct

answer while avoiding incorrect ones, enabling the model to focus on extracting critical local information and enhancing reasoning performance.

3) *Ablation of the design in VertexLang Topology Perceptor:* In this section, we perform ablation to analyze the advantages of the VertexLang Topology Perceptor compared to existing methods and the necessity of its internal designs.

**Advantage of VertexLang-based topology reconstruction at different sample scales.** We compare the performance of three global topology perception enhancement methods: TR-CoT captioning (NatureLang) [9], code-based reconstruction (CodeLang) [45], and our proposed VertexLang-based reconstruction across various sample scales. To ensure a fair comparison, we uniformly employ Qwen2.5-VL-3B for training, using the DynamicGT-RL strategy with a 50% GT proportion and edit distance as the reward signal. As summarized in Fig. 12 (a), in three geometric datasets, the total performance gains achieved through VertexLang training consistently surpass those of NatureLang in most scales and outperform CodeLang in all scales. We attribute this improvement to the removal of complex reconstruction code (as shown in Fig. 9), which enables the model to concentrate more effectively on global topology, thereby enhancing reasoning ability. Additionally, the simplified topology representation in VertexLang achieves a 20% reduction in training time compared to CodeLang under identical settings.

In the ablation study on the sample scale, we observe that as the sample scale increases, the performance of models trained with VertexLang demonstrates an upward trend. In contrast, NatureLang and CodeLang show a performance plateau and even decline when the data scale exceeds 10k. This finding suggests that expanding the scale of VertexLang-

TABLE V

ABLATION STUDY OF THE GEOFOCUS ON GEMMA3-4B. ‘TOPO’ DENOTES THE VERTEXLANG TOPOLOGY PERCEPTER. ‘LOCAL’ DENOTES THE CRITICAL LOCAL PERCEPTOR. BOTH MODULES ARE TRAINED ON SYNTHETIC DATA.

	Topo	Local	Geo3K	GeoQA	Formalgeo7k	Total
Gemma3-4B	✗	✗	30.6	42.6	37.0	110.2
	✓	✗	31.6	43.8	38.9	114.3 (4.1↑)
	✗	✓	31.8	44.3	38.4	114.5 (4.3↑)
	✓	✓	33.3	45.6	40.7	119.6 (9.4↑)

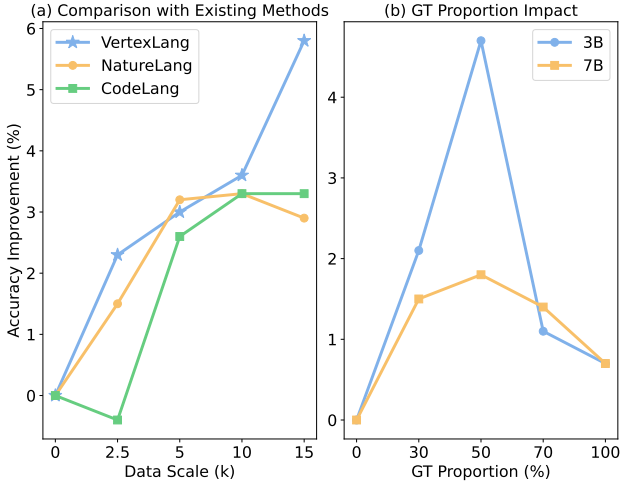


Fig. 12. (a) Comparison with existing methods at different sample scales. (b) Impact of GT ratio in DynamicGT-RL. The vertical axis shows the total performance improvement for Geo3K, GeoQA, and Formalgeo7K.

based synthetic data can effectively bridge the domain gap and further enhance the model’s performance in real-world reasoning tasks. To balance computational cost with evidential clarity, we cap our exploratory experiments at 15k samples. At this scale, VertexLang’s performance is still on an upward trajectory while the performance of competing methods has stopped rising, clearly demonstrating its superior scalability and data efficiency. We attribute this improvement to a deeper understanding of topological structures achieved by the VertexLang-trained model. This fundamental and general perceptual ability enhances the performance of out-of-domain GPS.

**Ablation of GT ratio in DynamicGT-RL.** We conducted an ablation to investigate the impact of the GT addition ratio on DynamicGT-RL. As illustrated in Fig. 12 (b), incorporating GT consistently improves performance compared to excluding it. Performance increases as the GT addition ratio rises, reaching a peak at a 50% threshold before gradually declining. These results support the hypothesis that an appropriate proportion of GT guides the model toward the correct optimization direction. In contrast, excessive reliance on GT may impair the model’s generalization ability.

**4) Ablation of effectiveness on different baselines:** We further validated the effectiveness of GeoFocus on Gemma3-4B [42], a recent open-source LMM that exhibits superior geometric reasoning compared with LMMs of similar size. As shown in Tab. V, integrating either module independently

TABLE VI

EXPLORING THE SEQUENTIAL DEPENDENCY BETWEEN THE PROPOSED MODULES. ‘1’ DENOTES THE VERTEXLANG TOPOLOGY PERCEPTER. ‘2’ DENOTES THE CRITICAL LOCAL PERCEPTOR.

Order	Geo3K	GeoQA	Formalgeo7k	Total
3B 2→1	26.5	32.9	15.8	75.2
3B 1→2	26.5	34.4	18.7	79.6 (4.4↑)
7B 2→1	39.3	47.0	35.9	122.2
7B 1→2	40.3	47.1	36.1	123.5 (1.3↑)

or combining both modules consistently led to performance improvements. This result demonstrates the universal effectiveness and robustness of the GeoFocus method across diverse model architectures.

**5) Exploring the sequential dependency between the proposed modules:** Considering humans tend to observe global structure first and then focus on critical local information when geometry reasoning, we employ the VertexLang Topology Perceptor to enhance the ability to perceive global topology structures during the initial stage. To validate the rationality of this training sequence, we investigate whether a definitive sequential order exists between global topology perception and critical local information extraction. As shown in Tab. VI, applying the VertexLang Topology Perceptor before the Critical Local Perceptor consistently performs better than the reverse order. This finding demonstrates the role of global topology perception in establishing the foundation for subsequent local information extraction. Reversing the sequence disrupts this natural learning progression, leading to weaker model performance. Therefore, in experiments, we begin by utilizing the VertexLang Topology Perceptor to establish a robust understanding of topological structures, followed by the Critical Local Perceptor to extract local information effectively.

### C. Performance Comparison

**1) Comparison with previous state-of-the-art:** Using GeoFocus, we developed two specialized GPS models, GeoFocus-3B and GeoFocus-7B, and evaluated them on three classic geometric benchmarks: Geo3K, GeoQA, and Formalgeo7K. As shown in Tab. VIII, GeoFocus-3B significantly surpasses many open-source general LMMs with larger parameter scales, such as InternVL-2.5-8B and Qwen2.5-VL-7B, demonstrating its efficiency and effectiveness for GPS. Furthermore, GeoFocus-7B outperforms the advanced geometric specialized model GeoUni by an average of 4.7%. These results demonstrate the potential and advantages of GeoFocus in GPS.

TABLE VII  
COMPARISON OF GENERALIZATION ABILITY OF OUT-OF-DOMAIN DATASETS.

Model	HALLUBENCH	WEMATH	MathVerse	MathVision	MathVista	ChartQA	Total	
3B	Baseline	60.5	51.7	34.3	21.3	56.4	73.2	297.4
	SFT	57.8	11.9	25.2	19.0	51.5	70.3	235.7
	GRPO	63.3	61.6	39.3	24.3	62.1	76.4	327.0
	GeoFocus	<b>64.7</b>	<b>62.5</b>	<b>39.4</b>	<b>24.5</b>	<b>63.9</b>	<b>76.6</b>	<b>331.6</b>
7B	Baseline	68.0	62.9	43.1	25.3	68.2	79.0	346.5
	SFT	57.5	20.2	15.4	18.5	55.6	71.1	238.3
	GRPO	68.7	68.9	45.7	27.7	72.1	81.3	364.4
	GeoFocus	<b>71.1</b>	<b>69.4</b>	<b>45.7</b>	<b>28.0</b>	<b>74.3</b>	<b>81.5</b>	<b>370.0</b>

TABLE VIII

TOP-1 ACCURACY (%) ON GEOMETRY PROBLEM SOLVING ON THE MAINSTREAM GEOMETRY DATASETS. \* REPRESENTS THE RESULTS FROM THE EXISTING PAPERS.

Model	Geo3K	GeoQA	Formalgeo7k
Closed-source LMMs			
Gemini 2.0 Flash [41]	58.2	69.1	36.5
GPT-4o [17]	34.6	34.0	36.7
Claude 3.7 [10]	31.1	26.9	24.0
Open-source LMMs			
Chameleon-7B [40]	3.9*	7.3*	5.9*
mPLUG-Owl2-7B [53]	12.7	13.0	6.6
Monkey-Chat-7B [21]	4.7	10.7	9.3
Deepseek-VL-7B [25]	5.2	12.2	5.8
InternVL-2.5-8B [5]	16.6	30.9	11.8
InternVL-3-2B [5]	31.1	31.2	17.4
InternVL-3-8B [5]	33.9	38.6	28.8
Gemma-3-4B [42]	30.6	42.6	37.0
Qwen2.5-VL-3B [1]	25.3	32.1	16.8
Qwen2.5-VL-7B [1]	39.4	44.4	35.6
Open-source Mathematical Geometry LMMs			
G-LLaVA-13B [12]	35.0*	20.1*	14.1*
GeoUni [6]	50.0*	66.7*	59.8*
GeoGen-SFT-3B [31]	38.6*	61.4*	-
GeoGen-SFT-7B [31]	46.3*	64.6*	-
GeoFocus-3B	50.4	64.3	55.4
GeoFocus-7B	<b>55.3</b>	<b>71.9</b>	<b>63.5</b>

## 2) Comparison of out-of-domain generalization ability:

To assess the robustness and generalization ability beyond the geometric domain, we further evaluate GeoFocus on the mathematical reasoning, chart (graph) reasoning, and hallucination datasets, as summarized in Tab. VII. Across all datasets, GeoFocus consistently outperforms symbolic reasoning models trained with supervised fine-tuning (SFT) or GRPO, and achieves an average improvement of 4.8% over the baseline. This improvement highlights the ability of GeoFocus to handle unknown data distributions and adapt effectively to new scenarios. Additionally, the performance improvement observed on the HALLUBENCH dataset highlights that GeoFocus plays a key role in mitigating the impact of visual illusions, allowing the model to maintain higher reasoning accuracy in complex

TABLE IX  
COMPARISON OF IMAGE RECONSTRUCTION ABILITY ON IN-DOMAIN AND OUT-OF-DOMAIN DATA.

Model	Connect. Acc.	Coord. Acc.
In-Domain	Qwen2.5-VL-3B	41.9
	+ VertexLang	62.5
	Qwen2.5-VL-7B	48.9
	+ VertexLang	68.9
Model	BLEU-4	Cons. CdlAcc
Out-of-Domain	Qwen2.5-VL-3B	32.6
	+ CodeLang	33.6
	+ VertexLang	34.0
	Qwen2.5-VL-7B	38.1
	+ CodeLang	33.0
	+ VertexLang	47.7

visual environments.

## V. DISCUSSION

This section analyzes the sources of GeoFocus’s performance gains along three dimensions: 1) in-domain and out-of-domain reconstruction, to quantify advances in topology perception and their generalization; 2) a series of tasks that incrementally raise visual perceptual demands by progressively removing explicit textual cues, to assess visual robustness; and 3) qualitative response analyses, to demonstrate tighter alignment between global topology and critical local structures.

### A. Image Reconstruction Performance

To explore the effectiveness of VertexLang in enhancing topology perception and reconstruction generalization, we compare in-domain and out-of-domain topology reconstruction performance of models trained with VertexLang. The in-domain test set comprises 500 VertexLang-based reconstruction instances, separate from the training set. As shown in the In-Domain section of Tab. IX, the model trained on VertexLang reconstruction samples achieved significant improvements, with an average increase of 20.3% in connection accuracy (Connect. Acc.) and 17.5% in coordinate accuracy (Coord. Acc.). We do not compare VertexLang and CodeLang on in-domain data, as the dataset only contains noise-free VertexLang annotations, while CodeLang annotations generated by LMMs may contain hallucination, making evaluation

**Question:**

Find XZ.

**Qwen2.5-VL-7B Output:**

<think>  $\triangle XYZ$  is a right triangle at  $W$ , so we can use the Pythagorean theorem. The length of  $YZ$  is  $5y - 6$ . The length of  $XY$  is  $18 + 2y$ . Using the Pythagorean theorem:  $XZ^2 = YZ^2 + XY^2$ . Substitute the given lengths:  $XZ^2 = (5y - 6)^2 + (18 + 2y)^2$ . Therefore,  $XZ = \sqrt{(29y^2 + 12y + 360)}$ . </think>  $\boxed{\sqrt{(29y^2 + 12y + 360)}}$

**GeoFocus-7B Output:**

<think> Since  $\triangle XYZ$  is divided by the altitude  $WX$ , it forms two right triangles,  $WXZ$  and  $WXY$ . We know that triangles  $WXZ$  and  $WXY$  are congruent triangles. We can use the given expressions for the sides:  $XZ = 5y - 6$ ,  $XY = 18 + 2y$ ,  $y = 8$ . Now,  $XZ = 5y - 6 = 5(8) - 6 = 40 - 6 = 34$ . </think>  $\boxed{34}$

**Question:**

Find  $m\angle CAM$

**Qwen2.5-VL-7B Output:**

<think> To find  $m\angle CAM$ , we need to use the properties of angles in a circle and the given information.  $\angle T$  subtended by the chord  $AC$  at the center  $M$  is given as  $28^\circ$ . Therefore,  $\angle CAM$  subtended by the same chord  $AC$  at point  $A$  on the circle is half of  $\angle T$ . So,  $m\angle CAM = \frac{1}{2} \cdot 28^\circ = 14^\circ$ . </think>  $\boxed{14^\circ}$

**GeoFocus-7B Output:**

<think> Given that  $\angle T = 28^\circ$  is an inscribed angle, the corresponding central  $\angle AOB$ , subtended by the same arc  $AB$ , is twice the measure of the inscribed angle.  $\angle AOB = 56^\circ$ . Since  $AM$  is a radius of the circle and is perpendicular to the  $TN$ , it bisects  $\angle AOB$ . Therefore,  $\angle CAM = 1/2 \cdot \angle AOB = 1/2 \cdot 56^\circ = 28^\circ$ . </think>  $\boxed{28^\circ}$

**Question:**

Find  $y$  in each figure.

**Qwen2.5-VL-7B Output:**

<think> To find the value of  $y$ , we need to use the property of vertical angles. Vertical angles are the angles opposite each other when two lines cross. They are always equal. The angles  $(8y + 2)^\circ$  and  $(25y - 20)^\circ$  are vertical angles. Therefore,  $8y + 2 = 25y - 20$ .  $y = \frac{22}{17}$ . </think>  $\boxed{\frac{22}{17}}$

**GeoFocus-7B Output:**

<think> The image shows two intersecting lines, creating four angles. The angles opposite each other are equal, and the adjacent angles add up to  $180^\circ$ . The two angles that are adjacent to each other are  $(8y + 2)^\circ$  and  $(25y - 20)^\circ$ . So, we can set up the equation:  $(8y + 2) + (25y - 20) = 180$ . The value is  $6$ . </think>  $\boxed{6}$

**Question:**

Find  $CD$  if  $AC = x - 3$ ,  $BE = 20$ ,  $AB = 16$ , and  $CD = y + 5$ .

**Qwen2.5-VL-7B Output:**

<think> To find the value of  $CD$ , we use the given relationships between segments. Since  $AB$  is a segment of  $AC$ , we can express  $AC$  as the sum of  $AB$  and  $BC$ . Since  $AC = x - 3$ ,  $CD = y + 5$ ,  $AB = 16$ , and  $BE = 20$ , we know that  $AC = CD + AB + BE$ . Substituting the expressions, we have  $(x - 3) + (y + 5) = 16 + 20$ . Simplifying,  $2x + 2 = 36$ , which gives  $2x = 34$ , and thus  $x = 17$ . Substituting  $x$  into  $CD = x - 5$ , we find  $CD = 17 - 5 = 12$ . </think>  $\boxed{12}$

**GeoFocus-7B Output:**

<think> Triangles  $\triangle ABC$  and  $\triangle ADE$  are similar because they share the same angles, satisfying the A similarity criterion. The ratio of corresponding sides of similar triangles is equal, so we can write the proportion:  $\frac{AC}{CD} = \frac{AB}{BE}$ . We have:  $\frac{x-3}{y+5} = \frac{16}{20}$ . So,  $x = 35$ ,  $CD = 35 - 5 = 40$ . </think>  $\boxed{40}$

Fig. 13. Qualitative example of reasoning. GeoFocus-7B produces more reliable multi-step reasoning responses by jointly enhancing global topology understanding and critical local perception. Red represents incorrect responses, and green represents correct responses

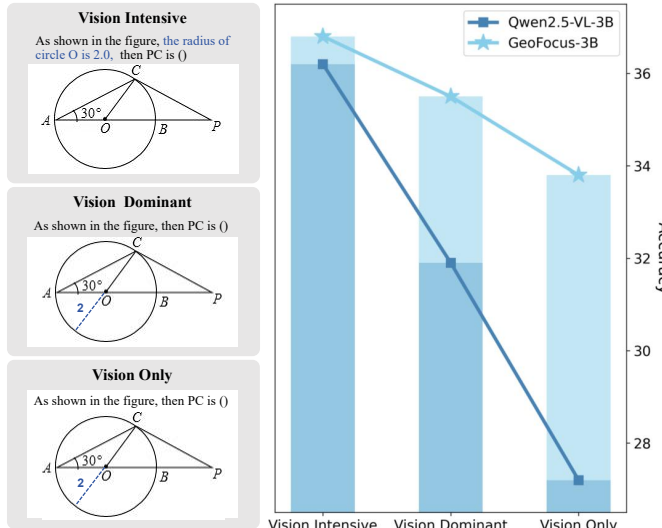


Fig. 14. Performance on MathVerse. The degree of visualization for problem-solving conditions increases progressively across ‘Vision Intensive’, ‘Vision Dominant’, and ‘Vision Only’.

unreliable. Instead, we focus the cross-format comparison on out-of-domain data. For out-of-domain evaluation, we used the Formalgeo7k test set, which reflects real-world reconstruction scenarios. As shown in the Out-of-Domain section of Tab. IX, models trained with CodeLang suffered a decline in structural accuracy (Cons. CdlAcc) due to hallucinations. In contrast, VertexLang demonstrated average improvements of 9.6% in BLEU-4 and 7.8% in Cons. CdlSAcc. These consistent gains demonstrate that training with VertexLang-based topology reconstruction effectively enhances the model’s topology perception accuracy. Moreover, the enhanced reconstruction ability

generalizes well to real-world reasoning images.

### B. Reducing Visual Perception Limitations

To explore whether the performance improvement brought by GeoFocus stems from alleviating limitations in visual perception, we conducted an evaluation following the metrics defined in MathVerse [57]. Specifically, we selected three types of problems from the MathVerse dataset, each exhibiting a different level of visualization dependence. As shown in Fig. 14: in the Vision Intensive setting, the problem text retains essential reasoning conditions; in the Vision Dominant setting, the text is further simplified, with all necessary conditions conveyed through visual input; in the Vision Only setting, all textual content, including the problem description, implicit attributes, and necessary conditions is conveyed solely through visual input.

As shown in Fig. 14, across all three categories, GeoFocus consistently outperforms the baseline. We further examined performance gaps as visualization complexity increases. The relatively small performance degradation in GeoFocus indicates stronger robustness and reduced sensitivity to shifts in the balance between textual and visual information. Moreover, the mitigated performance drop in the transition from Vision Dominant to Vision Only problems may stem from VertexLang’s enhancement of vertex-level annotation perception, which improves letter (e.g., point label) recognition within diagrams. This ability enables GeoFocus to infer problem-relevant textual cues even when they are presented exclusively via visual input.

### C. Reasoning Visualization

To better understand the performance improvements introduced by GeoFocus, we conducted a qualitative comparison

between the baseline model and our GeoFocus-7B model. Fig. 13 illustrates reasoning examples across different types of geometric images. The baseline model exhibits a primary limitation in GPS: it lacks an integrated perception of global geometric topology and critical local structures. This limitation leads to misinterpretations of triangle types, circle angle classifications, or collinear relationships (as shown in the left example of Fig. 13); and also causes failures in grounding geometric theories in concrete visual contexts (e.g., correctly identifying vertical angles, as in the first example on the right side of Fig. 13), even when the underlying definitions are recalled. In contrast, the responses generated by GeoFocus-7B demonstrate an accurate understanding of global topology and critical local structures, resulting in more accurate and reliable GPS performance.

#### D. Limitation

In the point-circle positional cases, conflicts may occur when explicit coordinates contradict topology constraints (e.g., the topology constraint indicates that the point lies on the circle, but its provided coordinates do not satisfy the circle equation), which leads to rendering failures. To ensure robustness, VertexLang prioritizes vertex coordinates over the positional constraints. However, this approach introduces small deviations for points that are intended to lie exactly on a circle, due to coordinate precision limitations. To mitigate downstream impact, we have designed a dedicated "On Circle" task type in Critical Local Perceptor to enhance the model's perception of point-circle positional relationships.

#### E. Future Exploration

GeoFocus combines theory-based local templates with the concise formal language VertexLang to improve the accuracy of planar geometric reasoning. Its dimension-independent abstract concepts enable a natural extension to solid geometry. Future work will focus on: (1) extending VertexLang to effectively represent three-dimensional geometric structures, including vertices, edges, and faces, thereby enabling modeling of spatial relationships; and (2) enhancing the Critical Local Perceptor to process three-dimensional visual perception for accurate reasoning in three-dimensional environments. Additionally, integrating spatial reasoning and volumetric analysis into the framework could unlock new possibilities for solving advanced geometric challenges, such as the analysis of polyhedra, curved surfaces, and transformations in three-dimensional space.

## VI. CONCLUSION

GeoFocus introduces thirteen theory-driven critical local templates that turn geometric local relations from incidental by-products of reasoning into explicit supervised learning targets. This shifts the paradigm from producing an answer with embedded rationale to a human-aligned strategy of first learning reusable local information extraction and then composing the reasoning chain. In parallel, VertexLang provides a

compact symbolic reconstruction of the global topology, giving a foundation for extracting the local information. Together, they form a two-stage perception process: (1) global structural abstraction and (2) targeted extraction of critical local cues. This also sets up a clear interface so the resulting local graph can later plug into a visual chain-of-thought, external geometry theorem libraries, or symbolic proof systems. We hope this work will provide valuable insights and references for future research.

## REFERENCES

- [1] Shuai Bai, Keqin Chen, Xuejing Liu, Jialin Wang, Wenbin Ge, Sibo Song, Kai Dang, Peng Wang, Shijie Wang, Jun Tang, et al. Qwen2.5-vl technical report. *arXiv preprint arXiv:2502.13923*, 2025.
- [2] Shihao Cai, Keqin Bao, Hangyu Guo, Jizhi Zhang, Jun Song, and Bo Zheng. Geogpt4v: Towards geometric multi-modal large language models with geometric image generation. In *Proceedings of the 2024 Conference on Empirical Methods in Natural Language Processing*, pages 750–766, 2024.
- [3] Jiaqi Chen, Tong Li, Jinghui Qin, Pan Lu, Liang Lin, Chongyu Chen, and Xiaodan Liang. Unigeo: Unifying geometry logical reasoning via reformulating mathematical expression. In *Proceedings of the 2022 Conference on Empirical Methods in Natural Language Processing*, pages 3313–3323, 2022.
- [4] Jiaqi Chen, Jianheng Tang, Jinghui Qin, Xiaodan Liang, Lingbo Liu, Eric Xing, and Liang Lin. Geoqa: A geometric question answering benchmark towards multimodal numerical reasoning. In *Findings of the Association for Computational Linguistics: ACL-IJCNLP 2021*, pages 513–523, 2021.
- [5] Zhe Chen, Weiyun Wang, Yue Cao, Yangzhou Liu, Zhangwei Gao, Erfei Cui, Jinguo Zhu, Shenglong Ye, Hao Tian, Zhaoyang Liu, et al. Expanding performance boundaries of open-source multimodal models with model, data, and test-time scaling. *arXiv preprint arXiv:2412.05271*, 2024.
- [6] Jo-Ku Cheng, Zeren Zhang, Ran Chen, Jingyang Deng, Ziran Qin, and Jinwen Ma. Geouni: A unified model for generating geometry diagrams, problems and problem solutions. *arXiv preprint arXiv:2504.10146*, 2025.
- [7] Francis DK Ching. *Architecture: Form, space, and order*. John Wiley & Sons, 2023.
- [8] Paul E Debevec, Camillo J Taylor, and Jitendra Malik. Modeling and rendering architecture from photographs: A hybrid geometry-and image-based approach. In *Seminal Graphics Papers: Pushing the Boundaries, Volume 2*, pages 465–474. Association for Computing Machinery, 2023.
- [9] Linger Deng, Yuliang Liu, Bohan Li, Dongliang Luo, Liang Wu, Chengquan Zhang, Pengyuan Lyu, Ziyang Zhang, Gang Zhang, Er-rui Ding, et al. R-cot: Reverse chain-of-thought problem generation for geometric reasoning in large multimodal models. *arXiv preprint arXiv:2410.17885*, 2024.
- [10] Maxim Enis and Mark Hopkins. From llm to nmt: Advancing low-resource machine translation with claude. *arXiv preprint arXiv:2404.13813*, 2024.
- [11] Daocheng Fu, Zijun Chen, Renqiu Xia, Qi Liu, Yuan Feng, Hongbin Zhou, Renrui Zhang, Shiyang Feng, Peng Gao, Junchi Yan, et al. Trustgeogen: Scalable and formal-verified data engine for trustworthy multimodal geometric problem solving. *arXiv preprint arXiv:2504.15780*, 2025.
- [12] Jiahui Gao, Renjie Pi, Jipeng Zhang, Jiacheng Ye, Wanjun Zhong, Yufei Wang, Lanqing HONG, Jianhua Han, Hang Xu, Zhenguo Li, and Lingpeng Kong. G-LLaVA: Solving geometric problem with multimodal large language model. In *The Thirteenth International Conference on Learning Representations*, 2025.
- [13] Tianrui Guan, Fuxiao Liu, Xiyang Wu, Ruiqi Xian, Zongxia Li, Xiaoyu Liu, Xijun Wang, Lichang Chen, Furong Huang, Yaser Yacoob, et al. Hallusionbench: An advanced diagnostic suite for entangled language hallucination and visual illusion in large vision-language models. In

*Proceedings of the IEEE/CVF Conference on Computer Vision and Pattern Recognition*, pages 14375–14385, 2024.

[14] Daya Guo, Dejian Yang, Haowei Zhang, Junxiao Song, Ruoyu Zhang, Runxin Xu, Qihao Zhu, Shirong Ma, Peiyi Wang, Xiao Bi, et al. Deepseek-r1: Incentivizing reasoning capability in llms via reinforcement learning. *arXiv preprint arXiv:2501.12948*, 2025.

[15] Yushi Hu, Weijia Shi, Xingyu Fu, Dan Roth, Mari Ostendorf, Luke Zettlemoyer, Noah A Smith, and Ranjay Krishna. Visual sketchpad: Sketching as a visual chain of thought for multimodal language models. *Advances in Neural Information Processing Systems*, 37:139348–139379, 2024.

[16] Kung-Hsiang Huang, Can Qin, Haoyi Qiu, Philippe Laban, Shafiq Joty, Caiming Xiong, and Chien-Sheng Wu. Why vision language models struggle with visual arithmetic? Towards enhanced chart and geometry understanding. *arXiv preprint arXiv:2502.11492*, 2025.

[17] Aaron Hurst, Adam Lerer, Adam P Goucher, Adam Perelman, Aditya Ramesh, Aidan Clark, AJ Ostrow, Akila Welihinda, Alan Hayes, Alec Radford, et al. Gpt-4o system card. *arXiv preprint arXiv:2410.21276*, 2024.

[18] Raisa Islam and Owana Marzia Moushi. Gpt-4o: The cutting-edge advancement in multimodal llm. In *Intelligent Computing-Proceedings of the Computing Conference*, pages 47–60. Springer, 2025.

[19] Simone Jablonski and Matthias Ludwig. Teaching and learning of geometry—A literature review on current developments in theory and practice. *Education sciences*, 13(7):682, 2023.

[20] Mehran Kazemi, Hamidreza Alvari, Ankit Anand, Jialin Wu, Xi Chen, and Radu Soricut. Geomverse: A systematic evaluation of large models for geometric reasoning. In *AI for Math Workshop@ ICML 2024*, 2024.

[21] Zhang Li, Biao Yang, Qiang Liu, Zhiyin Ma, Shuo Zhang, Jingxu Yang, Yabo Sun, Yuliang Liu, and Xiang Bai. Monkey: Image resolution and text label are important things for large multi-modal models. In *proceedings of the IEEE/CVF conference on computer vision and pattern recognition*, pages 26763–26773, 2024.

[22] Zhong-Zhi Li, Ming-Liang Zhang, Fei Yin, and Cheng-Lin Liu. Lans: A layout-aware neural solver for plane geometry problem. In *Findings of the Association for Computational Linguistics ACL 2024*, pages 2596–2608, 2024.

[23] Haotian Liu, Chunyuan Li, Qingyang Wu, and Yong Jae Lee. Visual instruction tuning. *Advances in neural information processing systems*, 36:34892–34916, 2023.

[24] Xiangyan Liu, Jinjie Ni, Zijian Wu, Chao Du, Longxu Dou, Haonan Wang, Tianyu Pang, and Michael Qizhe Shieh. Noisyrollout: Reinforcing visual reasoning with data augmentation. *arXiv preprint arXiv:2504.13055*, 2025.

[25] Haoyu Lu, Wen Liu, Bo Zhang, Bingxuan Wang, Kai Dong, Bo Liu, Jingxiang Sun, Tongzheng Ren, Zhuoshu Li, Hao Yang, et al. Deepseek-vl: Towards real-world vision-language understanding. *arXiv preprint arXiv:2403.05525*, 2024.

[26] Pan Lu, Hritik Bansal, Tony Xia, Jiacheng Liu, Chunyuan Li, Hannaneh Hajishirzi, Hao Cheng, Kai-Wei Chang, Michel Galley, and Jianfeng Gao. Mathvista: Evaluating mathematical reasoning of foundation models in visual contexts. In *The Twelfth International Conference on Learning Representations*, 2024.

[27] Pan Lu, Ran Gong, Shibiao Jiang, Liang Qiu, Siyuan Huang, Xiaodan Liang, and Song-chun Zhu. Inter-GPS: Interpretable geometry problem solving with formal language and symbolic reasoning. In *Proceedings of the 59th Annual Meeting of the Association for Computational Linguistics and the 11th International Joint Conference on Natural Language Processing (Volume 1: Long Papers)*, pages 6774–6786, 2021.

[28] Ruilin Luo, Zhuofan Zheng, Yifan Wang, Xinze Ni, Zicheng Lin, Songtao Jiang, Yiyao Yu, Chufan Shi, Ruihang Chu, Jin Zeng, et al. Ursu: Understanding and verifying chain-of-thought reasoning in multimodal mathematics. *arXiv preprint arXiv:2501.04686*, 2025.

[29] Ahmed Masyry, Xuan Long Do, Jia Qing Tan, Shafiq Joty, and Enamul Hoque. ChartQA: A benchmark for question answering about charts with visual and logical reasoning. In *Findings of the Association for Computational Linguistics: ACL 2022*, pages 2263–2279, 2022.

[30] Fanxu Meng, Haotong Yang, Yiding Wang, and Muhan Zhang. Chain of images for intuitively reasoning. *arXiv preprint arXiv:2311.09241*, 2023.

[31] Yicheng Pan, Zhenrong Zhang, Pengfei Hu, Jiefeng Ma, Jun Du, Jianshu Zhang, Quan Liu, Jianqing Gao, and Feng Ma. Enhancing the geometric problem-solving ability of multimodal llms via symbolic-neural integration. *arXiv preprint arXiv:2504.12773*, 2025.

[32] Kishore Papineni, Salim Roukos, Todd Ward, and Wei-Jing Zhu. Bleu: A method for automatic evaluation of machine translation. In *Proceedings of the 40th annual meeting of the Association for Computational Linguistics*, pages 311–318, 2002.

[33] Shuai Peng, Di Fu, Liangcai Gao, Xiuqin Zhong, Hongguang Fu, and Zhi Tang. Multimath: Bridging visual and mathematical reasoning for large language models. *arXiv preprint arXiv:2409.00147*, 2024.

[34] Shuai Peng, Di Fu, Yijun Liang, Liangcai Gao, and Zhi Tang. Geodrl: A self-learning framework for geometry problem solving using reinforcement learning in deductive reasoning. In *Findings of the Association for Computational Linguistics: ACL 2023*, pages 13468–13480, 2023.

[35] Runqi Qiao, Qiuna Tan, Guanting Dong, Minhui Wu, Chong Sun, Xiaoshuai Song, Zhuoma GongQue, Shanglin Lei, Zhe Wei, Miaoqian Zhang, et al. We-math: Does your large multimodal model achieve human-like mathematical reasoning? *arXiv preprint arXiv:2407.01284*, 2024.

[36] Minjoon Seo, Hannaneh Hajishirzi, Ali Farhadi, Oren Etzioni, and Clint Malcolm. Solving geometry problems: Combining text and diagram interpretation. In *Proceedings of the 2015 conference on empirical methods in natural language processing*, pages 1466–1476, 2015.

[37] Zhihong Shao, Peiyi Wang, Qihao Zhu, Runxin Xu, Junxiao Song, Xiao Bi, Haowei Zhang, Mingchuan Zhang, YK Li, Yang Wu, et al. Deepseekmath: Pushing the limits of mathematical reasoning in open language models. *arXiv preprint arXiv:2402.03300*, 2024.

[38] Sheng Shen, Liunian Harold Li, Hao Tan, Mohit Bansal, Anna Rohrbach, Kai-Wei Chang, Zhewei Yao, and Kurt Keutzer. How much can clip benefit vision-and-language tasks? In *International Conference on Learning Representations*, 2022.

[39] Wenhao Shi, Zhiqiang Hu, Yi Bin, Junhua Liu, Yang Yang, See Kiong Ng, Lidong Bing, and Roy Lee. Math-llava: Bootstrapping mathematical reasoning for multimodal large language models. In *Findings of the Association for Computational Linguistics: EMNLP 2024*, pages 4663–4680, 2024.

[40] Chameleon Team. Chameleon: Mixed-modal early-fusion foundation models. *arXiv preprint arXiv:2405.09818*, 2024.

[41] Gemini Team, Rohan Anil, Sebastian Borgeaud, Jean-Baptiste Alayrac, Jiahui Yu, Radu Soricut, Johan Schalkwyk, Andrew M Dai, Anja Hauth, Katie Millican, et al. Gemini: A family of highly capable multimodal models. *arXiv preprint arXiv:2312.11805*, 2023.

[42] Gemma Team, Aishwarya Kamath, Johan Ferret, Shreya Pathak, Nino Vieillard, Ramona Merhej, Sarah Perrin, Tatiana Matejovicova, Alexandre Ramé, Morgane Rivièvre, et al. Gemma 3 technical report. *arXiv preprint arXiv:2503.19786*, 2025.

[43] Shih-hung Tsai, Chao-Chun Liang, Hsin-Min Wang, and Keh-Yih Su. Sequence to general tree: Knowledge-guided geometry word problem solving. *arXiv preprint arXiv:2106.00990*, 2021.

[44] Ke Wang, Junting Pan, Weikang Shi, Zimu Lu, Houxing Ren, Aojun Zhou, Mingjie Zhan, and Hongsheng Li. Measuring multimodal mathematical reasoning with math-vision dataset. *Advances in Neural Information Processing Systems*, 37:95095–95169, 2024.

[45] Ke Wang, Junting Pan, Linda Wei, Aojun Zhou, Weikang Shi, Zimu Lu, Han Xiao, Yunqiao Yang, Houxing Ren, Mingjie Zhan, et al. Mathcoder-vl: Bridging vision and code for enhanced multimodal mathematical reasoning. *arXiv preprint arXiv:2505.10557*, 2025.

[46] Xing Wang, Hanwen Kang, Hongyu Zhou, Wesley Au, and Chao Chen. Geometry-aware fruit grasping estimation for robotic harvesting in apple orchards. *Computers and Electronics in Agriculture*, 193:106716, 2022.

[47] Yifan Wang, Liuchi Li, Douglas Hofmann, José E Andrade, and Chiara Daraio. Structured fabrics with tunable mechanical properties. *Nature*, 596(7871):238–243, 2021.

[48] Haoran Wei, Youyang Yin, Yumeng Li, Jia Wang, Liang Zhao, Jianjian Sun, Zheng Ge, Xiangyu Zhang, and Dixin Jiang. Slow perception: Let's perceive geometric figures step-by-step. *arXiv preprint arXiv:2412.20631*, 2024.

[49] Wenjun Wu, Lingling Zhang, Jun Liu, Xi Tang, Yaxian Wang, Shaowei Wang, and Qianying Wang. E-gps: Explainable geometry problem

solving via top-down solver and bottom-up generator. In *Proceedings of the IEEE/CVF Conference on Computer Vision and Pattern Recognition*, pages 13828–13837, 2024.

[50] Renqiu Xia, Mingsheng Li, Hancheng Ye, Wenjie Wu, Hongbin Zhou, Jiakang Yuan, Tianshuo Peng, Xinyu Cai, Xiangchao Yan, Bin Wang, et al. GeoX: Geometric problem solving through unified formalized vision-language pre-training. In *The Thirteenth International Conference on Learning Representations*, 2025.

[51] Shenzhi Wang et al. Yaowei Zheng, Junting Lu. Easyr1: An efficient, scalable, multi-modality rl training framework. <https://github.com/hiyouga/EasyR1>, 2025.

[52] Hiromi Yasuda, Philip R Buskohl, Andrew Gillman, Todd D Murphey, Susan Stepney, Richard A Vaia, and Jordan R Raney. Mechanical computing. *Nature*, 598(7879):39–48, 2021.

[53] Qinghao Ye, Haiyang Xu, Jiabo Ye, Ming Yan, Anwen Hu, Haowei Liu, Qi Qian, Ji Zhang, and Fei Huang. mplug-owl2: Revolutionizing multi-modal large language model with modality collaboration. In *Proceedings of the ieee/cvf conference on computer vision and pattern recognition*, pages 13040–13051, 2024.

[54] Yang Yue, Zhiqi Chen, Rui Lu, Andrew Zhao, Zhaokai Wang, Shiji Song, and Gao Huang. Does reinforcement learning really incentivize reasoning capacity in llms beyond the base model? *arXiv preprint arXiv:2504.13837*, 2025.

[55] Chengrui Zhang, Maizhen Ning, Zihao Zhou, Jie Sun, Kaizhu Huang, and Qifeng Wang. GeoSDF: Plane geometry diagram synthesis via signed distance field. *arXiv preprint arXiv:2506.13492*, 2025.

[56] Ming-Liang Zhang, Fei Yin, and Cheng-Lin Liu. A multi-modal neural geometric solver with textual clauses parsed from diagram. In *Proceedings of the Thirty-Second International Joint Conference on Artificial Intelligence*, pages 3374–3382, 2023.

[57] Renrui Zhang, Dongzhi Jiang, Yichi Zhang, Haokun Lin, Ziyu Guo, Pengshuo Qiu, Aojun Zhou, Pan Lu, Kai-Wei Chang, Yu Qiao, et al. Mathverse: Does your multi-modal llm truly see the diagrams in visual math problems? In *European Conference on Computer Vision*, pages 169–186. Springer, 2024.

[58] Renrui Zhang, Xinyu Wei, Dongzhi Jiang, Ziyu Guo, Yichi Zhang, Chengzhuo Tong, Jiaming Liu, Aojun Zhou, Shanghang Zhang, Peng Gao, et al. Mavis: Mathematical visual instruction tuning with an automatic data engine. In *The Thirteenth International Conference on Learning Representations*, 2025.

[59] Xiaokai Zhang, Na Zhu, Yiming He, Jia Zou, Qike Huang, Xiaoxiao Jin, Yanjun Guo, Chenyang Mao, Yang Li, Zhe Zhu, et al. Formalgeo: An extensible formalized framework for olympiad geometric problem solving. *arXiv preprint arXiv:2310.18021*, 2023.

[60] Zhuosheng Zhang, Aston Zhang, Mu Li, and Alex Smola. Automatic chain of thought prompting in large language models. *arXiv preprint arXiv:2210.03493*, 2022.

[61] Yaowei Zheng, Richong Zhang, Junhao Zhang, YeYanhan YeYanhan, and Zheyuan Luo. Llamafactory: Unified efficient fine-tuning of 100+ language models. In *Proceedings of the 62nd Annual Meeting of the Association for Computational Linguistics (Volume 3: System Demonstrations)*, pages 400–410, 2024.

[62] Qiji Zhou, Ruochen Zhou, Zike Hu, Panzhong Lu, Siyang Gao, and Yue Zhang. Image-of-thought prompting for visual reasoning refinement in multimodal large language models. *arXiv preprint arXiv:2405.13872*, 2024.

[63] Na Zhu, Xiaokai Zhang, Qike Huang, Fangzhen Zhu, Zhenbing Zeng, and Tuo Leng. Fgeo-parser: Autoformalization and solution of plane geometric problems. *Symmetry*, 17(1):8, 2024.

# Supplementary Material

## 1. CRITICAL LOCAL STRUCTURE TEMPLATES

Tab. XI provides a summary of the 13 categories of critical local structure templates covered by the proposed Critical Local Perceptor. The table is organized in three columns: Local Type, Question Template, and Answer (including positive and negative forms). The first five types (Angle Value, Angle Compare, Length Value, Length Compare, Area Compare) belong to Basic Measurement and focus on acquiring and comparing quantitative properties; the remaining eight (Shape Check, Bisector Check, Perp. Check, Parallel Check, Midpoint Check, On Circle, Perp. Foot Check, Collinearity) fall under Relational Reasoning and emphasize relationships among points, lines, and shapes. Each template provides both a correct answer and an incorrect answer (separated by a slash), enabling supervised positive–negative contrast.

TABLE X  
LOCAL COVERAGE COMPARISON OF GEOMETRIC DATASETS. ‘CLP’  
SHORT FOR CRITICAL LOCAL PERCEPTOR.

Local Type	CLP	CogAlign	GeoPep	MAVIS
Angle Value	✓	✗	✗	✗
Length Value	✓	✗	✗	✓
Quantity Check	✗	✓	✓	✗
Angle Compare	✓	✓	✗	✗
Length Compare	✓	✓	✗	✗
Area Compare	✓	✓	✗	✗
Slope Compare	✗	✓	✗	✗
Position Compare	✗	✓	✓	✗
Shape Check	✓	✓	✓	✓
Collinearity	✓	✗	✗	✗
Perp. Foot Check	✓	✗	✗	✗
On Circle	✓	✗	✗	✗
Intersect Check	✗	✓	✗	✗
Midpoint Check	✓	✗	✗	✗
Parallel Check	✓	✗	✗	✗
Bisector Check	✓	✗	✗	✗
Perp. Check	✓	✗	✗	✗
Local Coverage	<b>0.76</b>	<b>0.47</b>	<b>0.18</b>	<b>0.12</b>

## 2. CRITICAL LOCAL PERCEPTION COVERAGE

We compare the key local coverage of the Critical Local Perceptor with previous geometry perception question-answering pair generation methods, as shown in Tab. X. We divide all the critical local structure types contained in the methods into three categories: (a) numeric measurements (Angle Value, Length Value, Quantity Check); (b) relative comparisons (Angle Compare, Length Compare, Area Compare, Slope Compare, Position Compare); and (c) structural or constraint relations (Shape Check, Collinearity, Perp. Foot Check, On Circle, Intersect Check, Midpoint Check, Parallel Check, Bisector Check, Perp. Check). Critical Local Perceptor includes 13 core local perception tasks, achieving a local perception coverage of 76%. This is substantially higher than CogAlign [16] (47%), GeoPep [43] (18%), and MAVIS [58] (12%). The additional types in Critical Local Perceptor are mainly structural or constraint relations, which help the model

accurately extract local information related to geometric theory during reasoning. In contrast, CogAlign emphasizes basic angle and length measurements plus a limited subset of relation checks, while GeoPep and MAVIS cover fewer task categories.

## 3. DYNAMICGT-RL

During training using VertexLang-based reconstructed samples generated by the GeoVision Reconstructor (Tab. XII), we observed that supervised fine-tuning effectively injects task-specific knowledge but weakens the model’s generalization ability, limiting the application of perceptual skills from reconstruction tasks to reasoning tasks, and resulting in performance degradation when transferring topology perception to reasoning tasks. Reinforcement learning (RL) algorithms, while preserving reasoning generalization ability, provide limited improvement due to the model’s weak initial performance in image reconstruction, which makes RL struggle to identify optimization directions [54]. To accelerate convergence and improve training stability in the early stages, we propose DynamicGT-RL, which dynamically replaces the model-generated policy with ground truth (GT) to guide the model toward the correct optimization trajectory.

Specifically, for each question  $q$ , DynamicGT-RL samples a group of outputs  $\{o_1, o_2, \dots, o_U\}$  from the old policy  $\pi_{\theta_{old}}$  and then optimizes the policy model  $\pi_\theta$  by maximizing the following objective:

$$\begin{aligned} \mathcal{J}(\theta) = & \mathbb{E}_{q \sim P(Q), \{o_i\}_{i=1}^U \sim \pi_{\theta_{old}}(O|q)} \\ & \left[ \frac{1}{U} \sum_{i=1}^U \min \left( \frac{\pi_\theta(o_i|q)}{\pi_{\theta_{old}}(o_i|q)} \hat{A}_i(R), \right. \right. \\ & \left. \left. \text{clip} \left( \frac{\pi_\theta(o_i|q)}{\pi_{\theta_{old}}(o_i|q)}, 1 - \epsilon, 1 + \epsilon \right) \hat{A}_i(R) \right) \right. \\ & \left. - \beta \mathbb{D}_{KL} \left( \pi_\theta || \pi_{ref} \right) \right], \end{aligned} \quad (14)$$

$$\mathbb{D}_{KL} (\pi_\theta || \pi_{ref}) = \frac{\pi_{ref}(o_i|q)}{\pi_\theta(o_i|q)} - \log \frac{\pi_{ref}(o_i|q)}{\pi_\theta(o_i|q)} - 1, \quad (15)$$

where  $\epsilon$  and  $\beta$  are hyper-parameters.  $U$  represents the number of policies in a group, and  $\pi_{\theta_{old}}(O|q)$  does not participate in gradient updates.  $\hat{A}_i(R)$  denotes the advantage and  $R$  represents the reward function. The incorporation of GT influences  $\hat{A}_i(R)$  calculation in the following ways:

$$\hat{A}_i(R(P)) = \begin{cases} \frac{R(p_i) - \text{mean}(R(P_{model}))}{\text{std}(R(P_{model}))}, & \text{if } x \geq \tau, \\ \frac{R(p_i) - \text{mean}(R(P_{model} \cup P_{gt}))}{\text{std}(R(P_{model} \cup P_{gt}))}, & \text{if } x < \tau, \end{cases} \quad (16)$$

where  $p_i$  is a policy,  $P$  is a set of policies,  $x$  is a random number between 0 and 1, and  $\tau$  indicates GT replacement proportion. When the model fails to independently generate the correct solution, the GT policy provides a higher advantage, effectively guiding the model’s optimization direction. Conversely, as the model improves and begins generating correct solutions, the advantage of the GT policy gradually decreases, allowing the model to rely more on its own policy outputs without excessive dependence on the GT.

TABLE XI  
TEMPLATES IN THE CRITICAL LOCAL PERCEPTRON

Local Type	Question Template	Answer (chosen / rejected)
Angle Value	What is the measure of angle {A}?	Angle {A} measures {val} / {wrong_val} degrees.
Angle Compare	Which angle is greater between angle {A1} and {A2}?	Angle {A1} / {A2} is greater. Or: The two angles are identical.
	Are angles {A1} and {A2} equal?	Angle {A1} is equal to / not equal to angle {A2}.
Length Value	What is the length of segment {S}?	The length of {S} is {val} / {wrong_val}.
	What is the side length of the shape?	The side length is {val} / {wrong_val}.
	What is the radius of the circle?	The radius is {val} / {wrong_val}.
Length Compare	Which segment is longer: {S1} or {S2}?	{S1} / {S2} is longer. Or: The two segments are equal in length.
	Are segments {S1} and {S2} equal in length?	They are equal / not equal.
Area Compare	Which triangle has a greater area: triangle {T1} or {T2}?	Triangle {T1} / {T2} has a greater area.
	Do triangle {T1} and {T2} have equal areas?	They have equal / unequal areas.
Shape Check	Is the shape formed by {V} a {shape}?	The shape is / is not a {shape}.
	What type is quadrilateral {Q} (adjacent to {ref})?	It is a {correct_shape} / {wrong_shape}.
	What type is triangle {T}?	It is a {type} / {wrong_type}.
Bisector Check	Which line is the bisector of angle {A}?	Line {L} is / is not the bisector.
Perp. Check	Which line is perpendicular to line {L1}?	Line {L2} is / is not perpendicular to line {L1}.
Parallel Check	Is line {L2} parallel to {L1}?	Line {L2} is / is not parallel to line {L1}.
	Which line is parallel to line {L1}?	Line {L2} / {L3} is parallel to line {L1}.
Midpoint Check	Is point {P} the midpoint of segment {S}?	Point {P} is / is not the midpoint of segment {S}.
On Circle	Is point {P} on the circle?	Point {P} lies on / is not on the circle.
Perp. Foot Check	Is point {P} the foot of the perpendicular to line {L}?	Point {P} is / is not the foot.
Collinearity	Are points {P1}, {P2}, {P3} collinear?	Points are / are not collinear.

For the VertexLang-based image reconstruction task, we carefully design a Recon Reward  $R_{\text{recon}}$ , which consists of two verifiable reward functions: vertex coordinate accuracy reward  $R_{\text{coord}}$  and connectivity relationship accuracy reward  $R_{\text{conn}}$ . Vertex coordinate accuracy reward is assessed by calculating the Euclidean distance between the model-predicted coordinates and the corresponding GT coordinates. Based on the distance  $d(v)$  and predefined thresholds  $\tau_1$  and  $\tau_2$ , the score for each vertex is defined as follows:

$$\text{score}(v) = \begin{cases} 1.0, & \text{if } d(v) \leq \tau_1 \\ 0.5, & \text{if } \tau_1 < d(v) \leq \tau_2 \\ 0.0, & \text{if } d(v) > \tau_2 \end{cases} \quad (17)$$

The final vertex coordinate accuracy score is the average of all vertex scores:

$$R_{\text{coord}} = \frac{1}{|\mathcal{V}|} \sum_{v \in \mathcal{V}} \text{score}(v), \quad (18)$$

where  $|\mathcal{V}|$  denotes the total number of vertices. Connectivity relationship accuracy reward is measured using the F1 score  $R_{\text{conn}}$ , which compares the model-predicted edge set  $E_{\text{model}}$  with the GT edge set  $E_{\text{gt}}$ . The final reward score is computed by the vertex coordinate accuracy score and the connectivity relationship accuracy score:

$$R_{\text{recon}} = 0.5 * R_{\text{coord}} + 0.5 * R_{\text{conn}}. \quad (19)$$

TABLE XII  
IMAGE RECONSTRUCTION TRAINING METHOD ABLATION EXPERIMENT.  
'SL' REPRESENTS SUPERVISED LEARNING. 'RL' REPRESENTS REINFORCEMENT LEARNING.

	Training	Geo3K	GeoQA	Formalgeo7k	Total
3B	Baseline	25.3	32.1	16.8	74.2
	+ SL	25.4	31.6	14.9	71.9
	+ RL	25.3	32.4	16.7	74.4
	+ DynamicGT-RL	25.4	33.8	17.3	76.5
7B	Baseline	39.4	44.4	35.6	119.4
	+ SL	38.9	43.5	34.4	116.8
	+ RL	39.6	46.3	35.0	120.9
	+ DynamicGT-RL	39.8	46.6	36.0	122.4

where  $R_{\text{recon}}$  is substituted into Eq. 16 to perform the corresponding calculation.

As shown in Tab. XII, DynamicGT-RL selectively incorporates GT guidance while primarily relying on autonomous outputs, allowing the model to progressively acquire reconstruction skills without compromising reasoning ability. By improving topology understanding, this approach further enhances reasoning accuracy.